SYNERGY
PUBLISHING PTE. LTD.

Volume 5
Issue 02
October 2021

ISSN 2591-7110(Print) 2591-7129(Online)

Modern Electronic Technology

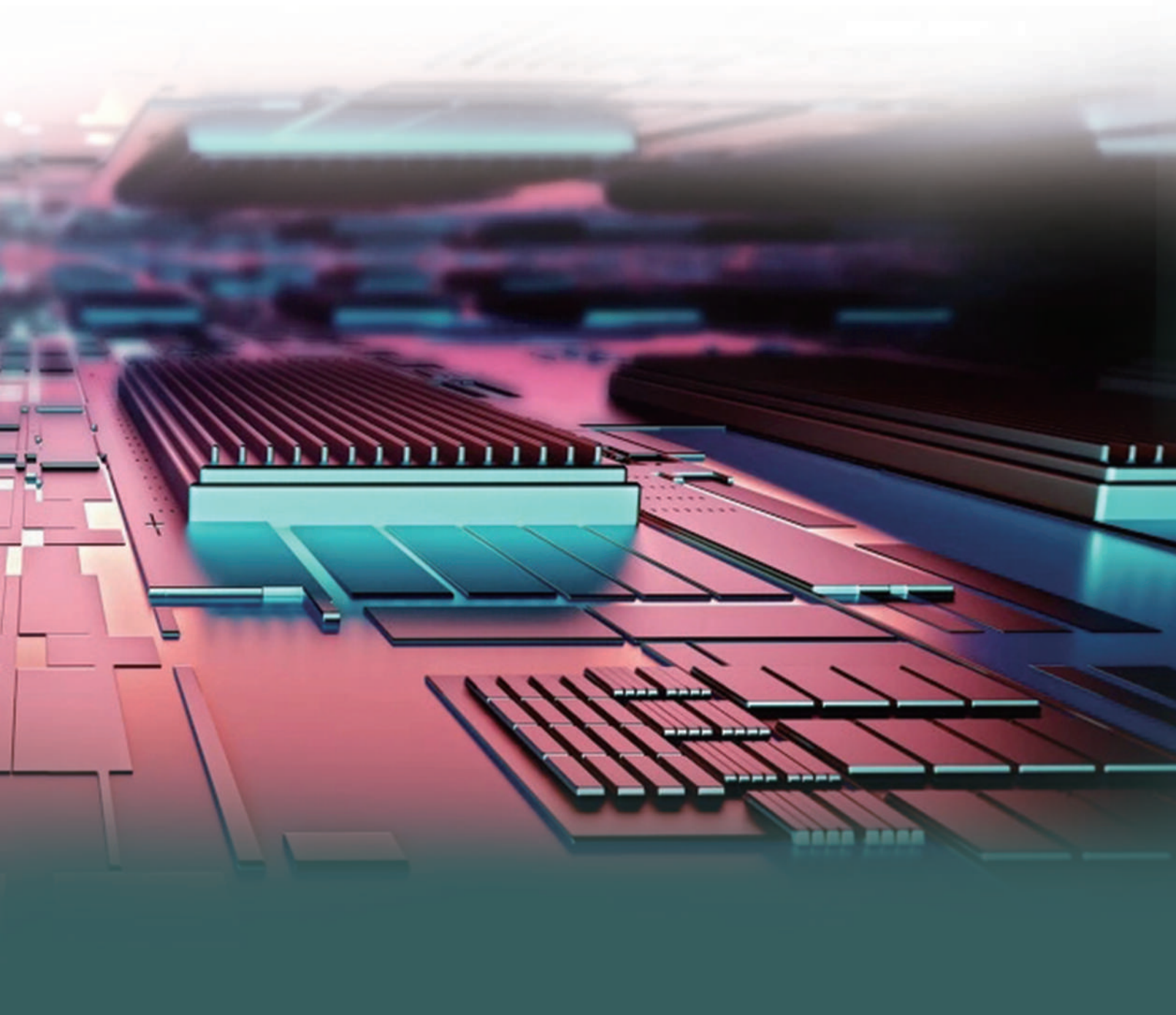

Modern Electronic Technology

Aims and Scope

Modern Electronic Technology (MET) is an open access, peer-reviewed scholarly journal which aims to publish original research articles, reviews and short communications that covers all area of electronic engineering technology. MET emphasizes on publishing high quality papers, as well as aims to provide a source of information and discussion platform for engineers, researchers, and electronic professionals worldwide.

Subject areas suitable for publication include, but are not limited to the following fields:

- Microelectronics
- Nanoelectronics
- Electronic Materials Technology
- Structure and Nature of Semiconductor
- Digital Technology
- Automation System

Publishing Cycle

Quarterly

Journal Homepage

http://ojs.s-p.sg/index.php/met

Key Features

- Open Access
- High Academic Level Editorial Board
- Easy and Fast Submissions
- Double Blind Peer Review
- Rapid Online Publication of Articles upon Acceptance
- Outlet for Academic Institutions and Industry

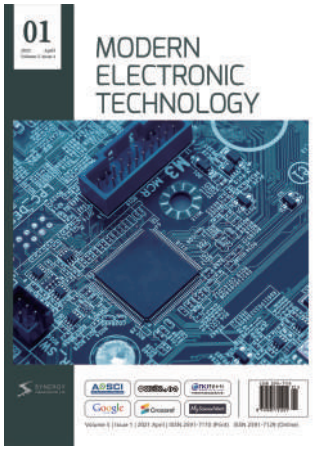

Volume 5 Issue 2 · October 2021
ISSN 2591-7110 (Print) ISSN 2591-7129 (Online)

Synergy Publishing Pte.Ltd.

E-Mail: contact@s-p.sg
Official Website: www.s-p.sg
Address: 12 Eu Tong Sen Street, #07-169, Singapore 059819

CONTENTS

SYNERGY PUBLISHING PTE. LTD

Modern Electronic Technology

https://ojs.s-p.sg/index.php/met

Research on Direct Torque Control of Permanent Magnet Synchronous Motor for New Energy Vehicles

Zhenzhou Niu* **Xiaopeng Li**

Tianjin University of Technology and Education, Tianjin, 300222, China

ARTICLE INFO

Article history
Received: 20 April 2021
Revised: 27 April 2021
Accepted: 18 October 2021
Published Online: 25 October 2021

Keywords:
Motor control strategy
Control principle
Direct torque control

ABSTRACT

This article introduces the control principle, technical status and two commonly used motor control schemes of permanent magnet synchronous motors for new energy vehicles. Direct torque control is selected as the research object, and its advantages and disadvantages with vector control are analyzed. A Simulink simulation model was established according to the control principle.

1. Introduction

The core technology of new energy vehicles is the "Three electric", including power batteries, drive motors and motor controllers. Power batteries are the energy source of the entire new energy vehicle. The drive motor is the power core of the vehicle. The motor controller can control the speed, torque and direction of the drive motor according to the received instructions. Currently, power batteries have limited capacity and are expensive. New energy vehicle drive motors can be divided into DC motors, AC asynchronous motors, permanent magnet synchronous motors and switched reluctance motors. Among them, AC asynchronous motors and permanent magnet synchronous motors are the most widely used in new energy vehicles. However, in China, permanent magnet synchronous motors occupy a dominant market position by virtue of their high power-density and small size, etc. According to data from the Ministry of Industry and Information Technology, as of June 2019, the domestic installed capacity of drive motors was 650,000, of which permanent magnet synchronous motors accounted for 99% of the market. Before a major breakthrough in battery technology, how to improve the power and endurance of new energy vehicles will be the primary problem faced by new energy vehicle designers. And high-efficiency motor control technology will be one of the ways to solve this series of problems.

2. Principles of Motor Control

The drive motor system of new energy vehicle is a

**Corresponding Author:*
Zhenzhou Niu,
Tianjin University of Technology and Education, Tianjin, 300222, China;
Email: 635924238@qq.com

 https://doi.org/10.26549/met.v5i2.6898

combination of the drive motor, the drive motor controller and the auxiliary devices necessary for its work. The drive motor system is the main executive system in the driving of new energy vehicles, and its driving characteristics determine the main performance indicators of the car. The high-voltage power output by the power battery is distributed by the high-voltage control box, and then the high-voltage DC power is inverted into three-phase AC power by the drive motor controller. Finally, the drive motor converts electrical energy into mechanical energy [1]. The high-voltage transmission line is shown in Figure 1.

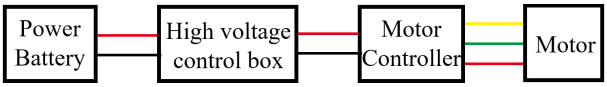

Figure 1. Electric vehicle high-voltage transmission line diagram

The drive motor is mainly composed of stator, rotor, sensor and shell. The rotor of a permanent magnet synchronous motor is generally composed of an iron core and a permanent magnet. According to the installation position of the permanent magnet on the rotor, the rotor type can be divided into surface mount type and embedded type. When a three-phase alternating current is applied to the stator of the motor, a stable rotating magnetic field is generated inside the motor. The magnetic field of the rotor is subjected to the electromagnetic force of the stator magnetic field, so that the rotor rotates synchronously with the stator magnetic field to generate electromagnetic torque.

The motor controller is mainly composed of the main control unit, drive module, power module, housing and cooling system. The main control unit is the "brain" of the motor controller, with underlying software and control algorithms written inside, which can realize motor control based on accelerator pedal signals, motor resolver signals, CAN signals, etc. The function of the drive module is to output a pulse width modulation signal to control the power module after receiving the signal from the main control unit. The power module is generally an insulated gate bipolar transistor (IGBT), which can realize the inversion from direct current to alternating current by controlling the on and off of the IGBT, and can also rectify the alternating current recovered during braking into direct current. IGBT is a composite full-controlled voltage-driven power semiconductor device composed of a bipolar transistor and an insulated gate field effect transistor, which works in a saturated state and an off state. When the IGBT is working in a saturated state, the circuit is turned on, and when the IGBT is working in an off state, the circuit is turned off. The motor control structure is shown in Figure 2.

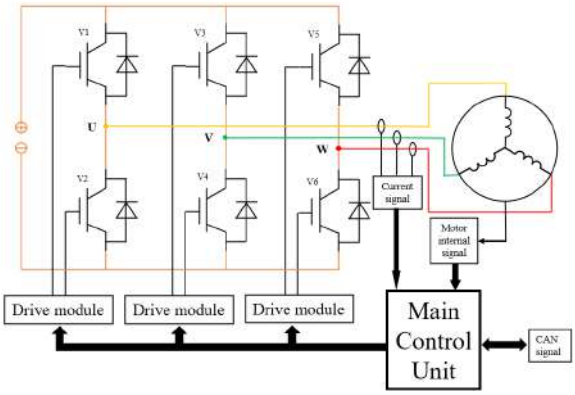

Figure 2. Motor control structure diagram

3. Current Statue of Motor Control Technology

Since the 21st century, with environmental, climate and energy issues, governments of various countries have issued a series of policies to promote the development of electric vehicles. This has allowed the production and sales of electric vehicles to grow steadily, and it has also driven the rapid development of motor control technology.

Motor control technology is divided into hardware part and software part, and its development follows the development of microelectronics, computer, materials science and other disciplines [2]. The hardware part is composed of microcontroller, drive module, insulated gate bipolar transistor (IGBT), sensor and protection circuit. The software part consists of motor control algorithm, motor status detection and safety monitoring, rotor position decoding algorithm and so on.

The core of the hardware part is mainly the microcontroller and IGBT. For the microcontroller, the working environment inside the car is relatively harsh, and its reliability and safety requirements are also higher. Therefore, the microcontroller must be certified by the reliability standard AEC-Q100, the quality management standard ISO/TS16949, and the functional safety standard ISO26262 before it can be used in the car. In 2019, NXP accounted for the largest proportion of the global automotive chip market, reaching 14%, and Infineon was second only to NXP, accounting for 11%.

Most of the manufacturers of electric vehicle power modules are concentrated in Western countries and Japan. Among them, Infineon, Mitsubishi Electric, Semikron, Fuji Electric and other companies have launched products specifically for automotive-grade IGBTs. My country's BYD, STARPOWER and other companies have also entered the fast lane in the IGBT industry. Among them, STARPOWER ranked 8th in the global market share of IGBT modules in 2018, and it is also the only Chinese enterprise that has entered the top ten in the world. In terms of IGBT technical strength, BYD released IGBT

https://doi.org/10.26549/met.v5i2.6898

4.0 in 2018, which is equivalent to the fifth-generation technology in the world. STARPOWER has developed to the sixth-generation technology, and the highest international level is the current level of Mitsubishi Electric. It can be regarded as 7.5 generation technology.

The core of the software part is mainly the control algorithm of the motor. The commonly used control methods of permanent magnet synchronous motors are vector control and direct torque control. Both of these control methods can realize the high dynamic performance of the motor and variable frequency speed regulation. But because of the characteristics of these two control methods, they have their own different best application scenarios.

Vector control, proposed by Hasse of Darmstadt University of Technology in the late 1960s. The main idea of this control method is that the excitation current and armature current of the reference DC motor are perpendicular to each other, are not coupled, and can be controlled independently. Vector control decouples the stator current in the three-phase coordinate system into direct-axis and quadrature-axis components through coordinate transformation, that is, the excitation current and the armature current. Then the current is controlled, so that the permanent magnet synchronous motor has a control performance similar to that of a DC motor.

Direct Torque Control (DTC) is another new type of high-efficiency variable frequency speed regulation technology after vector control technology. In the mid-1980s, Professor Depenbrock of Ruhr University in Germany proposed this control scheme [3], The main idea of this control method is to decouple the stator voltage and current in the three-phase coordinate system into the voltage and current in the rectangular coordinate system through coordinate transformation, and then calculate and control the flux linkage and torque of the motor.

Although direct torque control appeared more than ten years later than vector control, there is no difference in its control mode, and the basic control structure of the two is similar. Compared with vector control, direct torque control has the advantages of simple control structure, fast control calculation speed, and strong robustness. Its disadvantage is that the control performance of the motor is poor when the motor is operating at low speed. In addition, when the motor runs for a period of time, the temperature of the motor rises, and its stator resistance changes accordingly, which leads to a large error in the flux linkage estimation and a large torque ripple [4].

4. Principle of Direct Torque Control

In direct torque control, the angle between the stator flux linkage and the rotor flux linkage is the torque angle, and the magnitude of the motor torque and the flux linkage amplitude is controlled by controlling the torque angle. Assume that the rotor flux is rotating counterclockwise. When the motor torque and flux linkage amplitude are less than the preset value, you need to select a voltage vector that is not greater than 90° counterclockwise than the rotor flux linkage to increase the motor torque and flux linkage amplitude. When the motor torque is greater than the preset value and the flux linkage amplitude is less than the preset value, it is necessary to select a voltage vector not greater than 90° clockwise than the rotor flux linkage to reduce the motor torque and increase the flux linkage amplitude. When the motor torque is less than the preset value and the flux linkage amplitude is greater than the preset value, it is necessary to select a voltage vector that is greater than 90° and not greater than 180° counterclockwise than the rotor flux linkage to increase the motor torque and reduce the flux linkage amplitude. When the motor torque and flux linkage amplitude are greater than the preset value, it is necessary to select a voltage vector that is greater than 90° clockwise than the rotor flux linkage and not greater than 180° to reduce the motor torque and flux linkage amplitude.

The traditional direct torque control of a three-phase permanent magnet synchronous motor can be roughly divided into four modules, namely the flux estimation and torque calculation module, the hysteresis control module, the pulse width signal modulation module, and the speed loop control module.

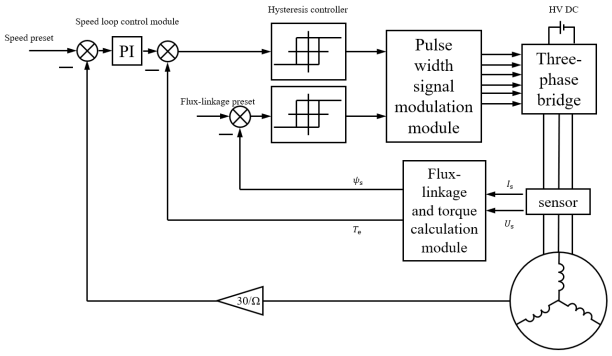

Figure 3. Principle of Direct Torque Control

In direct torque control, the three-phase voltage and current of the motor need to be Clarke transformed to convert them into voltage and current in a two-phase static coordinate system. The coordinate transformation formula is as follows.

$$I_\alpha = I_a - cos\left(\frac{\pi}{3}\right) I_b - cos\left(\frac{\pi}{3}\right) I_c \quad (1)$$

$$I_\beta = sin\left(\frac{\pi}{3}\right) I_b - sin\left(\frac{\pi}{3}\right) I_c \quad (2)$$

$$U_\alpha = U_a - cos\left(\frac{\pi}{3}\right) U_b - cos\left(\frac{\pi}{3}\right) U_c \quad (3)$$

$$U_\beta = sin\left(\frac{\pi}{3}\right)U_b - sin\left(\frac{\pi}{3}\right)U_c \quad (4)$$

In the flux estimation and torque calculation module, the flux vector estimation equation and torque calculation equation of the motor are as follows [5].

$$\Psi_s = \int (u_s - R_s i_s)\, dt \quad (5)$$

$$T_e = \frac{3}{2}\frac{P_n}{L_d}|\Psi_s|\Psi_f \sin\delta + \frac{3(L_d - L_q)}{4L_d L_q}|\Psi_s|^2 \sin 2\delta \quad (6)$$

Where Ψ_s is the stator flux linkage, $\mathrm{u_s}$ is the stator voltage, $\mathrm{R_s}$ is the stator resistance, $\mathrm{i_s}$ is the stator current, T_e is the electromagnetic torque of the motor, P_n is the number of pole pairs, L_d is the direct-axis inductance, L_q is the quadrature-axis inductance, Ψ_f is Rotor flux, $\delta$is the torque angle, that is the angle between the stator flux and the rotor flux. For surface mount permanent magnet synchronous motors, the direct axis inductance is equal to the quadrature axis inductance, so the torque calculation equation is as follows.

$$T_e = \frac{3}{2}\frac{P_n}{L_d}|\Psi_s|\Psi_f \sin\delta \quad (7)$$

The three-phase bridge of the motor controller inverts direct current into alternating current, and the upper and lower switching devices of the same bridge arm cannot be turned on at the same time at any time. Remember that the upper bridge arm is turned on as 1, and the lower bridge arm is turned on as 0. Then the three-phase bridge has 8 switch states, which are 000, 100, 110, 010, 011, 001, 101, 111, named U_0-U_7 in order, of which 6 non-zero vectors are distributed 60° apart in space. The vector diagram of the space voltage is shown in Figure 4(a).

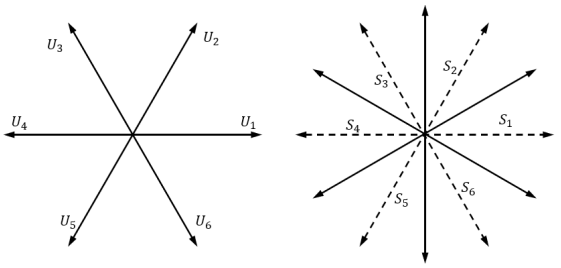

Figure 4. (a) Voltage vector diagram (b) Sector distribution diagram

The direction of the stator voltage vector determines the direction of the stator flux increase. Inputting different voltage vectors can make the motor flux reach the predetermined trajectory. Taking the angular bisector of two adjacent basic non-zero voltage vectors as the boundary, the space is divided into 6 sectors, as shown in Figure 4(b). Determine the sector where the stator flux vector is located, select different voltage vectors to change the flux amplitude and electromagnetic torque. Take the flux linkage vector in sector S_1 as an example, the rotation direction of the motor is counterclockwise, and the influence of different space voltage vectors on it is shown in the following table.

The flux linkage and torque are compared with the expected value, and the difference is controlled by the hysteresis controller. Record the increase output as 1, and the decrease output as 0. When the difference does not exceed the tolerance value set by the hysteresis controller, the last signal output is used; When the difference exceeds the tolerance value set by the hysteresis controller and the actual value is less than the expected value, the output signal is 1; When the difference exceeds the tolerance value set by the hysteresis controller and the actual value is greater than the expected value, the output signal is 0. According to the influence of the 6 space voltage vectors on the flux linkage and torque in each sector, the optimal switching table of the permanent magnet synchronous motor is established, as shown in the following table.

5. Simulation

According to the principle of three-phase permanent magnet synchronous motor direct torque control, a simulation model is built in the MATLAB/Simulink 2020b environment, as shown in Figure 5. The simulation uses the built-in Simulink three-phase permanent magnet synchronous motor model, and the switching device of the three-phase bridge arm is six insulated gate bipolar transistor. Its parameters are set as follows: DC voltage is 311V, motor rotor type is surface mount type, stator resistance R_s is 1.2Ω, stator inductance L_d and L_q is 8.5×10^{-3}H, rotor flux ψ_f is 0.175Wb, the moment of inertia J is $8 \times 10^{-4} kg \cdot m^2$.

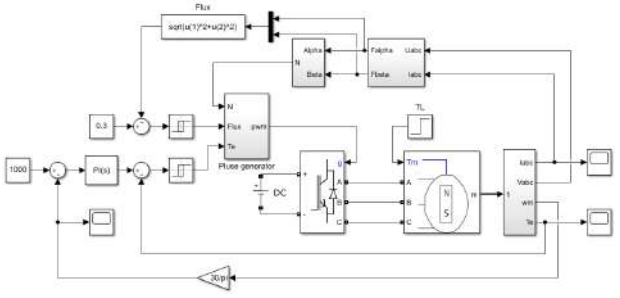

Figure 5. Permanent magnet synchronous motor direct torque control simulation model

In the flux estimation module, the three-phase voltage and three-phase current of the permanent magnet synchronous motor are transformed into the voltage and current in the rectangular coordinate system, and the α and β components of the flux linkage vector are calculated and output according to formula (5). The flux estimation module is shown in Figure 6.

https://doi.org/10.26549/met.v5i2.6898

Table 1. The influence of different space voltage vectors on the flux linkage in sector S_1

Basic voltage vector	U_1	U_2	U_3	U_4	U_5	U_6
Influence on the amplitude of the flux linkage	Dramatic increase	Increase	Decrease	Sharp decrease	Decrease	Increase
Influence on electromagnetic torque		Increase	Decrease		Decrease	Decrease

Table 2. PMSM traditional direct torque control optimal switch table

Flux linkage	Torque	First sector	Second sector	Third sector	Fourth sector	Fifth sector	Sixth sector
1	1	U_2	U_3	U_4	U_5	U_6	U_1
	0	U_6	U_1	U_2	U_3	U_4	U_5
0	1	U_3	U_4	U_5	U_6	U_1	U_2
	0	U_5	U_6	U_1	U_2	U_3	U_4

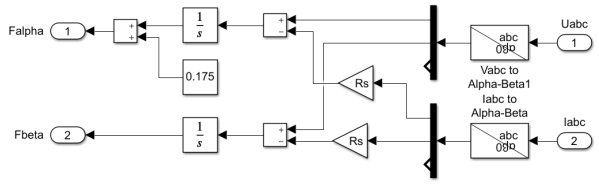

Figure 6. Flux link estimation module

According to the composite signal composed of the α and β components of the flux linkage vector, the phase angle of the composite signal is calculated to output the angle of the flux linkage vector and determine the sector where the flux linkage vector is located. The sector determination module is shown in Figure 7.

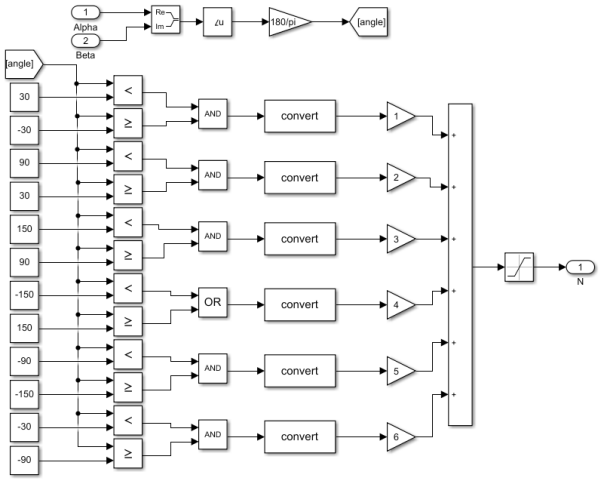

Figure 7. Sector Judgment Module

The calculated sector and the flux linkage and torque after hysteresis control are input to the pulse width signal modulation module, and six PWM signals are generated according to the traditional direct torque control optimal switch table to control the IGBT of the three-phase bridge arm. Pulse width signal modulation module is shown in Figure 8.

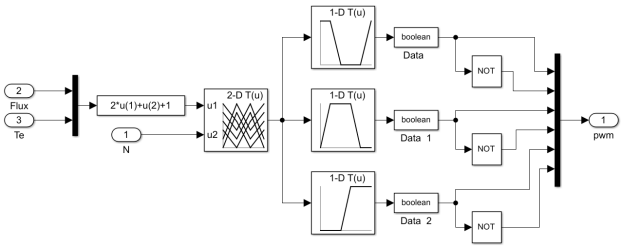

Figure 8. Pulse width signal modulation module

The simulation configuration uses the fixed-step ode23tb algorithm, the fixed-step size is10^{-5}, and the simulation time is 1s. The motor speed is set to 1000rpm, the expected value of the stator flux linkage is 0.3Wb, and a load torque of 10Nm is suddenly added at 0.5s. The simulation result of the direct torque control of the three-phase permanent magnet synchronous motor is shown in Figure 9.

6. Conclusions

From the analysis of the simulation results, although the direct torque control has a certain overshoot in the speed and torque at the beginning, it still has a good dynamic response performance, which can meet the needs of motor control performance. However, in the actual motor operation process, the traditional direct torque control has many problems. For example, it is difficult to accurately control under low-speed conditions, the switching frequency of the inverter is not constant, the larger flux linkage and torque ripple and the high-frequency noise caused by it, etc. In response to these problems, its control process needs to be optimized. For example, the voltage vector is subdivided and the zero-voltage vector added to the switch table, using the method of space voltage vector modulation, introduce sliding mode control, fuzzy control, etc. into traditional direct torque control, in order to solve various problems existing in traditional direct torque

 https://doi.org/10.26549/met.v5i2.6898

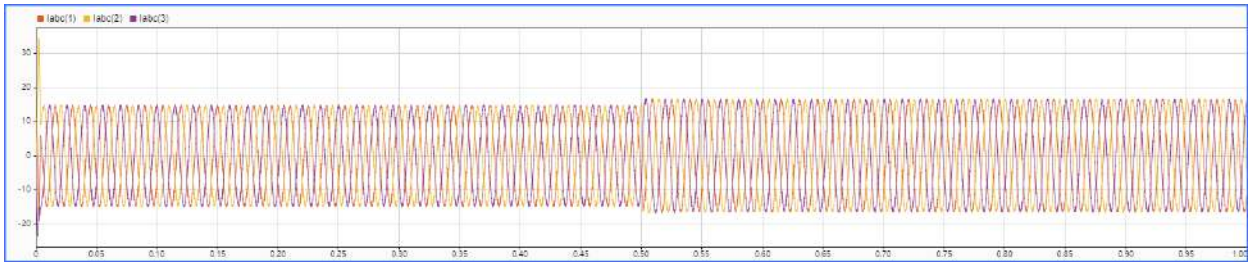

(a) Current waveform

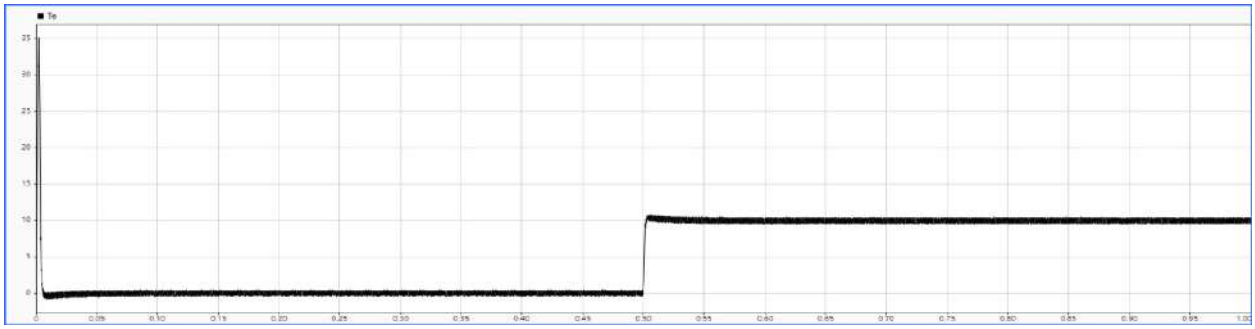

(b) Torque waveform

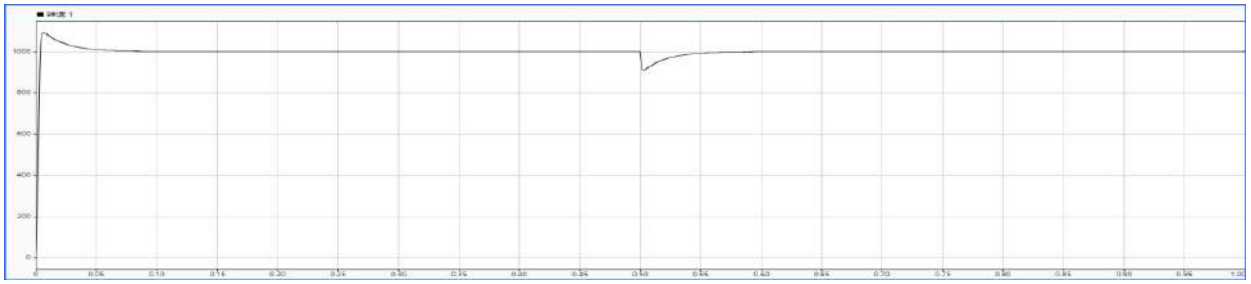

(c) Speed waveform

Figure 9. Permanent magnet synchronous motor direct torque control simulation results

control, make its control more precise, run more efficient, and more robust.

References

[1] Nie Guanghui. Control Principle of Electric Vehicle Motor Controller [J]. Modern Industrial Economy and Informationization,2019,9(11):56-57.

[2] Huang Qi, Chen Xiang, Luo Ling, etc. Design of Permanent Magnet Synchronous Motor Controller for Electric Vehicle [J]. Electric Machines and Control Application,2019,46(10):84-91.

[3] Su Dandan, Li Haodong, Yin Yanzhou, etc. Improved model predictive direct torque control of permanent magnet synchronous motors [J]. Journal of Hebei University (Natural Science Edition),2020,40(06):666-672.

[4] Pan Mian, Lin Hui, Li Xungen, etc. Improved model predictive direct torque control for permanent magnet synchronous motor [J]. Electri c Machines and Control,2020,24(07):102-111.

[5] Yufeng Luo, Gongquan Tan, Chang Su. Direct Torque Control of Permanent Magnet Synchronous Motor Based on Sliding Mode Variable Structure[J]. Open Access Library Journal, 2019, 6(9):1-10.

https://doi.org/10.26549/met.v5i2.6898

SYNERGY PUBLISHING PTE. LTD

Modern Electronic Technology

https://ojs.s-p.sg/index.php/met

A 4-element Rectangular Microstrip Patch Antenna Array

Demou Cao* **Zhihan Zhang** **Kai Kang** **Qiaoyu Wang**

Electrical and Computer Systems Engineering Department, Monash University, Melbourne, Victoria, Australia

ARTICLE INFO

Article history
Received: 21 May 2021
Revised: 28 May 2021
Accepted: 18 October 2021
Published Online: 25 October 2021

Keywords:
Antenna gain
Antenna efficiency
Directivity
Return loss
Transmission loss
Far-field
Radiation pattern

ABSTRACT

Patch antennas are small in size and suitable for microwave transmission, so they are widely used in small portable wireless devices. Multiple patch antennas are connected together to form an array antenna. Compared with the patch antenna, the array antenna has a higher directivity gain and can achieve better transmission performance. In this project, I will test the single patch antenna first, and then move to 2×1 antenna array. Finally, built a 2×2 antenna array, test and record their performance respectively.

1. Introduction

CST Microwave Studio is a powerful electromagnetic field simulation software. In this design project, I built a 2×2 antenna array with cooper and FR-4 materials, then tune the parameters and test the model to achieve a quite good performance at my assigned frequency(2.7411GHz).

2. Background

Directional property of an antenna is defined in term of 'directive gain'. Directive gain is ratio of the normalised power intensity in a particular direction to the average normalised power intensity such as from an isotropic radiator [1,2]. Directivity is the maximum of directive gain: $D_{\max} = \frac{P_n(\theta,\phi)_{\max}}{P_n(\theta,\phi)_{ave}} = \frac{1}{P_n(\theta,\phi)_{ave}} = \frac{4\pi}{\Omega_p}$. Antenna gain = directivity times efficiency: $G = eD_{\max}$. The antenna efficiency is defined as: $\eta = \frac{P_{rad}}{P_{rad} + p_{diss}} = \frac{R_r}{R_r + R_l}$, where R_l is loss resistance, R_r is radiation resistance. The total efficiency of an antenna is the radiation efficiency multiplied by the impedance mismatch loss of the antenna, when connected to a transmission line or receiver (radio or transmitter). The E-plane and H-plane are reference planes for linearly polarized waveguides, antennas and other microwave devices [3,4].

For a linearly-polarized antenna, E-plane is the plane containing the electric field vector and the direction of maximum radiation. The electric field or "E" plane determines the polarization or orientation of the radio wave [5,6]. H-plane is the plane containing the magnetic field vector and the direction of maximum radiation [7]. In a radio antenna's radiation pattern, the main lobe is the

**Corresponding Author:*
Demou Cao,
Electrical and Computer Systems Engineering Department, Monash University, Melbourne, Victoria, Australia;
Email: 2126828166@qq.com

 https://doi.org/10.26549/met.v5i2.6998

lobe containing the higher power. This is the lobe that exhibits greater field strength [8]. The beamwidth of the antenna is the width of the main lobe, usually specified by the half power beam width (HPBW), the angle encompassed between the points on the side of the lobe where the power has fallen to half (-3 dB) of its maximum value [9]. The antenna bandwidth is defined as the band of frequency over which the performance of the antenna remains within an acceptable limit. Reflection coefficient S11 is a ratio of the reflected power and incident power [8-10]. Through return loss in dB, we can calculate S11 by using: $S11=10^{-\frac{RL}{10}}\times 100\%$. The greater value of S11, the worse transmission performance.

3. Simulation Results

3.1 Patch Antenna Design

3.1.1 Initial Parameter Setting

Before built the model, we need set the value of all parameter we will use. First, calculating the value of necessary parameters should do first. MATLAB code is shown in Figure 1, and all of the parameters are setting as shown in Table 1 [11].

```
e_r = 4.3;
tan_sig = 0.019;
h = 1.6e-3;
e0 = 8.854e-12;
mu0 = 4*pi*(10^-7);
f_test = 2.4711e9;
z0 = 50;

W_patch = (1/(2*f_test*sqrt(e0*mu0)))*sqrt(2/(e_r+1));
e_reff = (((e_r+1)/2) + (e_r-1)*(1+ (12*h/W_patch))^(-1/2)/2);
det_L = h*0.412*((e_reff+0.3)*(W_patch/h+0.264))/((e_reff-0.258)*(W_patch/h+0.8));
L_patch = (1/(2*f_test*sqrt(e_reff)*sqrt(e0*mu0))) - (2*det_L);

A = ((z0/60)*sqrt((e_r+1)/2)) + (((e_r-1)/(e_r+1))*(0.23 + (0.11/e_r)));
B = (377*pi)/(2*z0*sqrt(e_r));
e = log(B-1) + 0.39 - (0.61/e_r);
e1 = ((e_r-1)/(2*e_r))*e;
SmallRatio = ((8*exp(A))/(exp(2*A)-2));
BigRatio = (2/pi)*(B -1 - log((2*B)-1) + e1);

if SmallRatio <= 2
 W_line = SmallRatio*h;
else
 W_line = BigRatio*h;
end
```

Figure 1. MATLAB code for calculate parameters

Table 1. Initial parameters

Parameter	Value (mm)
Board Width (BW)	55
Board Length (BL)	55
Copper Thickness (t)	0.017
Substrate Thickness (h)	1.6
Patch Width (PW)	37.3
Patch Length (PL)	28.9
Feed Line Width (FW)	3.14
Slot Length (y0=$\frac{1}{3}PL$)	9.63
Free space Wavelength (λ_0)	121.4
ad	0.7

3.1.2 Optimize S_{11}

First we should use parameter sweep to step change the y0 to change the S_{11}, make sure S_{11} is better than -30 dB around 2.4711 GHz. Then we fix the value of y0, and tune the PL value to shift the peak of S_{11} plot at resonant frequency. The finally goal in this stage is to achieve that the S_{11} at resonant frequency is greater than -30 dB [12-15]. My S_{11} result is -44.015 dB and shown in Figure 2. The final value of slot length is y_0=8.03, the patch length is PL=28.2mm and achieve the S11 is -44.015dB at frequency is 2.4764GHz. Also, the directivity is 6.384dBi which was improved by optimizing the slot length and patch length, and better than 6dBi [12-15]. The far field result is shown in Figure 3. The Polar result of 90 degree and 0 degree are shown in Figure 4 and Figure 5 respectively.

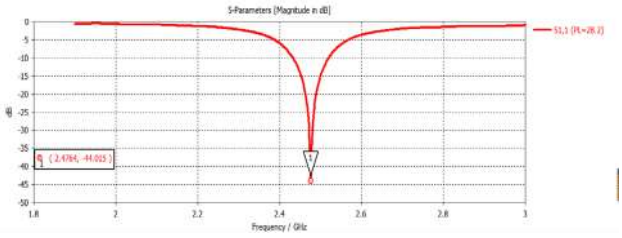

Figure 2. Patch antenna S_{11} result by tuning y0 and PL

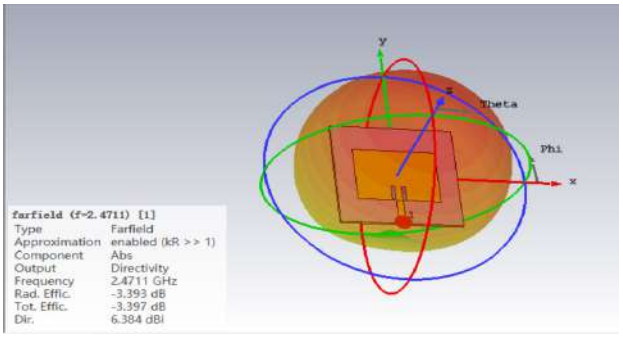

Figure 3. Patch antenna Directivity result in farfield

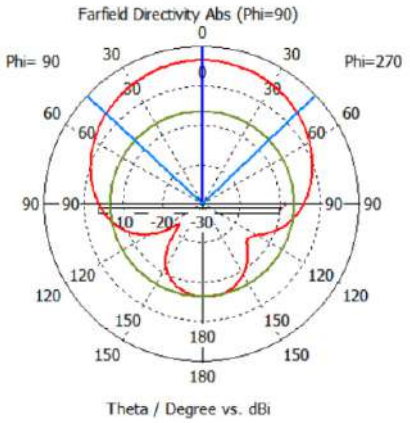

Figure 4. Farfield Directivity (Phi=90)

https://doi.org/10.26549/met.v5i2.6998

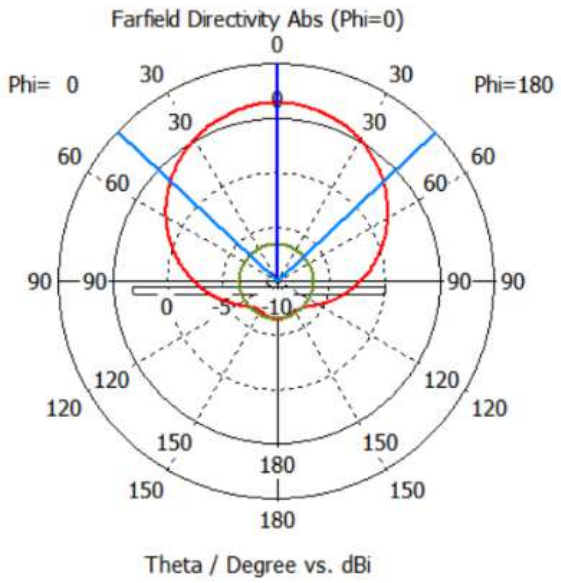

Figure 5. Farfield Directivity (Phi=0)

3.2 2×1 Antenna Array Design

At beginning of this part, a 3dB power divider should be constructed. First set the ground plane and substrate length as d=ad×wavelength to make sure the size of power divider will match the 2×1 Antenna array size. Through the Macros function in CST to calculate the 70.7Ω transmission line width and length[13]. The transmission line width is 1.64mm and line length is 17.279mm. Then, use one and two 50Ω line connected with the transmission line as input line and output line respectively. The plot of S-parameters is shown in Figure 6.

After built the power divider, connected it with 2×1 antenna array and repeat the step of tuning as previous part. Through my optimizing, the Directivity of the 2×1 antenna array is 9.705dBi, which is better than 9dBi [12-15] and shown in Figure 7. The S_{11} is -49.207dB at 2.4742GHz and the Realized Gain is 5.579dBi (better than 5dB) shown in Figure 8 and Figure 9 respectively.

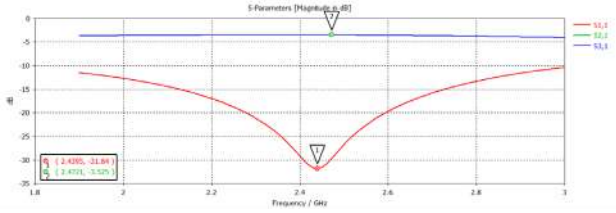

Figure 6. S-parameters plot of Power Divider

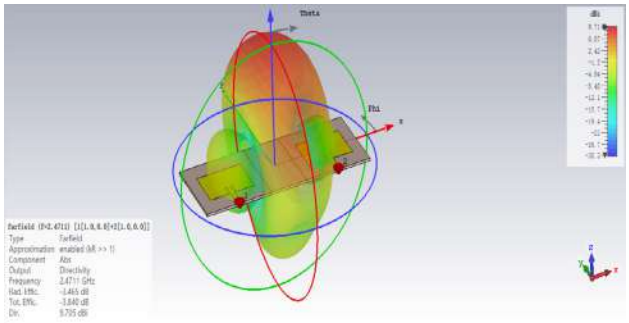

Figure 7. Two Patch Antenna Directivity result in far-field

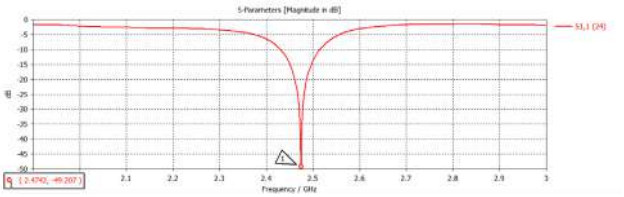

Figure 8. 2×1Antenna array S11 result

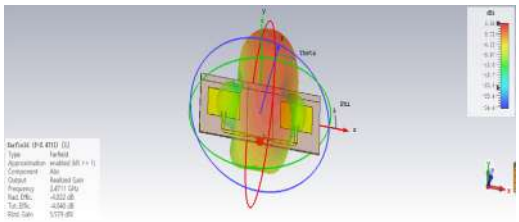

Figure 9. 2×1Antenna array Realized Gain result in far-field

3.3 2×2 Antenna Array Final Integration

This is the final part of designing, and I have built a completed 2×1 Antenna array, to integrate a 2×2 Antenna array, translate and copy the 2×1 Antenna array with a distance ($0.7\lambda_0$ [13]) first, then copy the Power Divider and add it. Also, antenna tuning is necessary to ensure the S11 is better than -30dB at resonant frequency(2.4711GHz±10MHz) and achieve the Realized Gain is greater than 7dB. The tuning results of S11 are -41.402dB at 2.472GHz, which is shown in Figure 10. Meanwhile, the Realized Gain is 8.013dBi and shown in Figure 11.

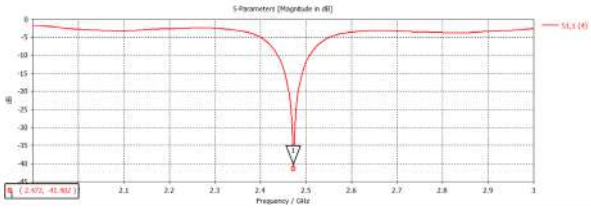

Figure 10. 2×2 Antenna array S11 result in far-field

 https://doi.org/10.26549/met.v5i2.6998

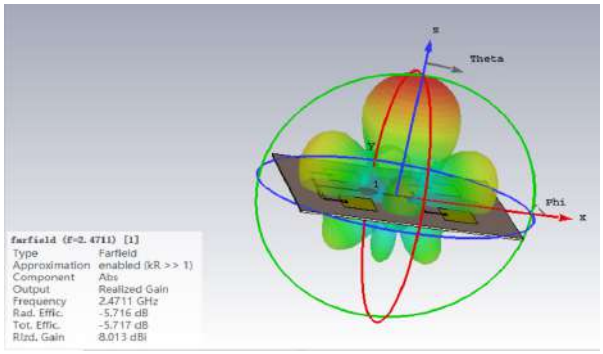

Figure 11. 2×2 Antenna array Realized Gain result in farfield

For final integration, delete the upper labelled transmission line in the Y direction, construct a meandered transmission line, and the dimensions should be defined as Figure 12 shows. Finally, observing the far-field Polar plot of Directivity at Phi=90 when altering the phase shift as 22.5°, 45° and 90° in this case. The result is shown in Figure 13. All the simulation parts are finished at this point.

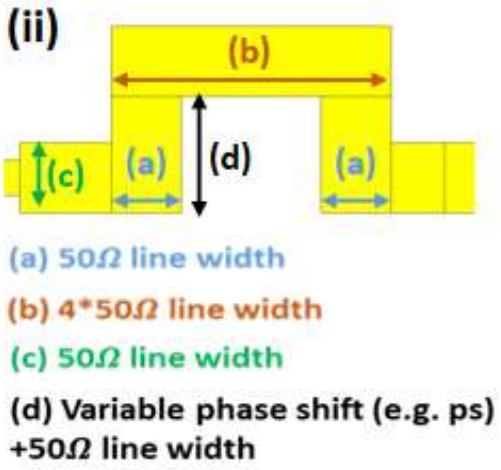

Figure 12. Parameters of meandered line setting

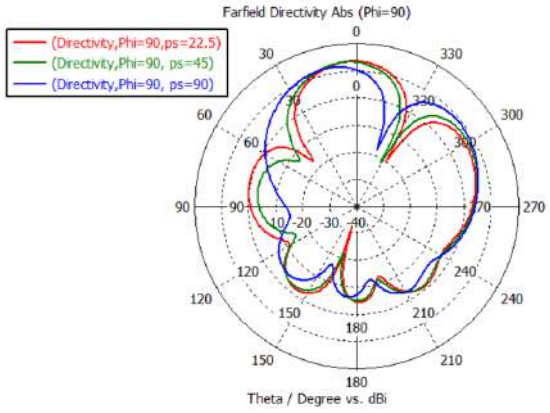

Figure 13. Farfield result with phase shift =22.5°, 45° and 90°

4. Measured Results

In this part, measured S_{11} and antenna gain of a 2-element array and a 4-element array antenna with MiniVNA equipment. The measurement of antenna gain is calculated by Friis Transmission Equation. Figure 14 shows when connect with DET, and S_{11} is -24.44 dB at 2.4333 GHz. Figure 15 illustrates connect with DUT, S_{11} is -25.27 dB at 2.4327 GHz. Figure 16 shows S_{21} of 2-element antenna array is -15.15 dB at 2.4474 GHz.

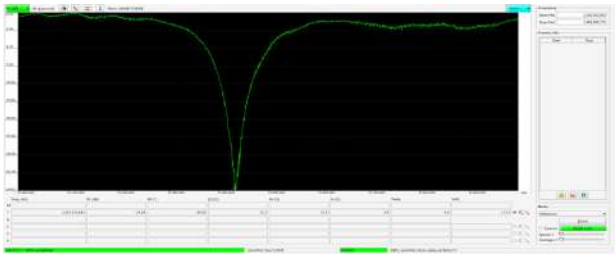

Figure 14. S_{11} vs Frequency connect with DET

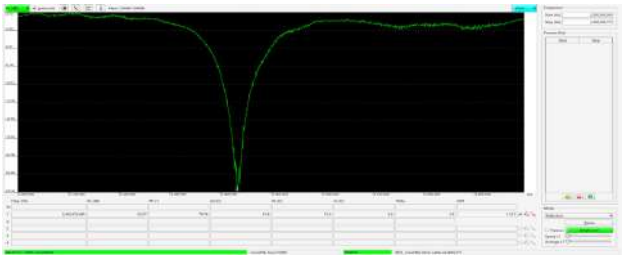

Figure 15. S_{11} vs Frequency connect with DUT

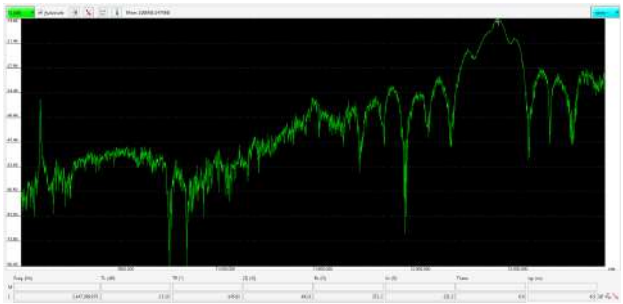

Figure 16. S_{21} vs Frequency of 2-elements antenna array

The gain of the 2×1 antenna array is calculated using the Friis Transmission Equation [16], $G_{Array}(\mathrm{dB}) = \frac{1}{2}\{32.45 + 20\log_{10} 2.4474 + 20\log_{10} 0.2 - 15.15 + 1.5\} = 6.2973$ dB

Now I measure the return loss and transmission loss of Power Divider and 4-elements antenna array with power divider. Figure 17 shows the plot of return loss with frequency of power divider, and at 2.4305GHz, S_{11}= -18.60dB, Figure 18 shows the return loss of 4-element array with power divider is -15.69 dB at 2.3599GHz.

https://doi.org/10.26549/met.v5i2.6998

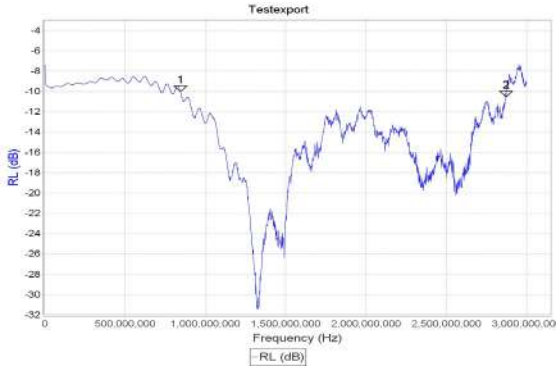

Figure 17. S_{11} vs Frequency of power divider

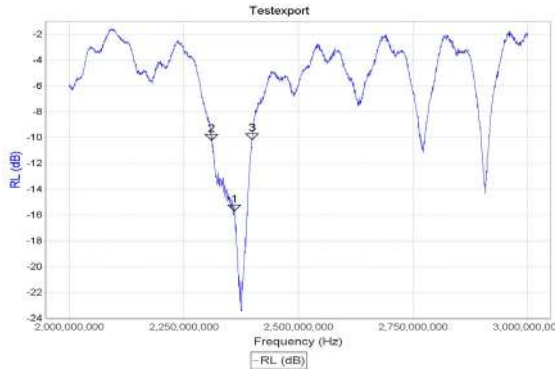

Figure 18. S_{11} vs Frequency of 4-element array with power divider

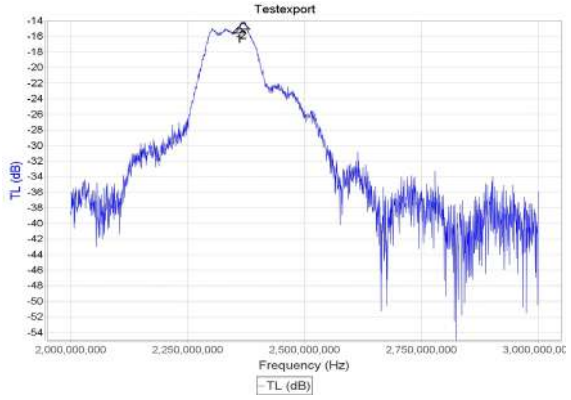

Figure 19. S_{21} vs frequency of 4-element array with power divider

The gain of the 4-element antenna array with power divider is calculated using the Friis Transmission Equation [16], $G_{Array}(\mathrm{dB}) = \frac{1}{2}\{32.45 + 20\log_{10} 2.3599 + 20\log_{10} 0.2 - 14.72 + 1.5 - 1.5\} = 6.3542$ dB

The radiation pattern of antenna array is measured by rotating 5°every time between -90° and 90° to obtain the value of S_{21} for both E-plane and H-plane.

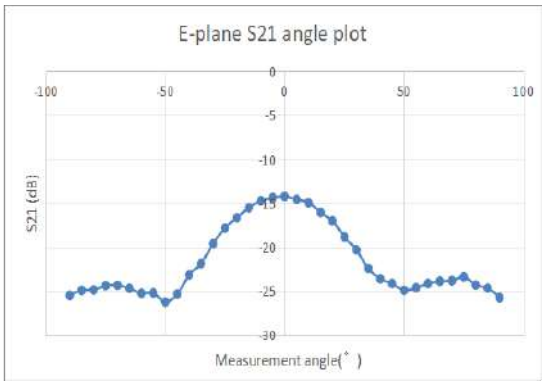

Figure 20. E-plane radiation pattern

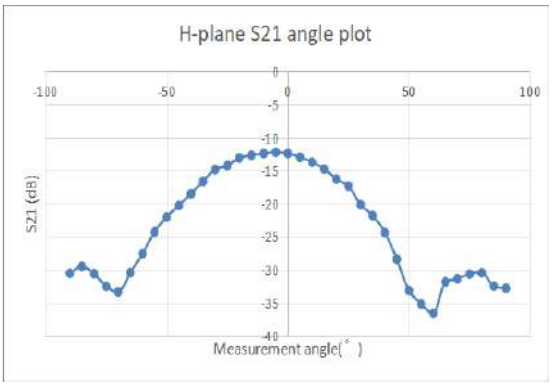

Figure 21. H-plane radiation pattern

5. Conclusions

Overall, the slot length and patch length are the critically important parameters which have a significant effect on antenna performance. With the increase of the number of patch antennas, we can see that the gain and directivity of antennas is increasing. Therefore, increasing the number of patch antennas can achieve better transmission performance, and achieving more usages in our life. In my design, I also achieve the 2×2 antenna array has benefits over the single patch antenna as theory. From the observation of transmission loss and realized gain both in simulation results and measured results, the 2×2 antenna array has a higher gain and lesser transmission loss.

It is also clear that, for the 2×2 antenna array design, we can find the simulation result on CST platform is better than the measured result on MiniVNA. Probably, the reason is in practical, there are more loss exist, and also the microstrip patch antennas generally have quite narrow bandwidth which result in very sensitive to the environment setting and the accuracy of placement. In CST platform, the line loss is constant and materials are all have a uniform density, which is an ideal situation for antenna, so the result is better. When measuring the transmission loss of the antenna array, the requirements

 https://doi.org/10.26549/met.v5i2.6998

for frequency matching are very high, because the antenna bandwidth we use is very narrow, and the same frequency must be ensured to achieve 100% signal transmission.

References

[1] Balanis, C. A. (2016). Antenna theory (4th ed.). Hoboken: Wiley.

[2] Collin, R., & Zucker, Francis J. (1969). Antenna theory (Inter-university electronics series ; v. 7). New York: McGraw-Hill.

[3] Fang, D. G. (2017). Antenna Theory and Microstrip Antennas. Taylor and Francis.

[4] Huang, Yi, & Boyle, Kevin. (2008). Antennas (1st ed.). Hoboken: Wiley.

[5] Thourel, L. (1960). The antenna. Chapman & Hall.

[6] Chen, C., Institution of Engineering Technology, & EuCap 2017. (n.d.). A Special Antenna Gain Measurement Technique / 2017 March 23.

[7] Gliddon, C., & Monash University. (1973). Antenna Radiation Pattern Measurements Using Model Aircraft.

[8] Lee, Kyoungmin M, Kang, Inwoong, Park, Jaedon, & Kim, Moonil. (2019). Antenna pattern analysis using S−parameters for strongly coupled dipole arrays. Microwave and Optical Technology Letters, 61(5), 1337-1340.

[9] Farouq, Mohamed, Serhir, Mohammed, & Picard, Dominique. (2016). Antenna Far-Field Assessment From Near-Field Measured Over Arbitrary Surfaces. IEEE Transactions on Antennas and Propagation, 64(12), 5122-5130.

[10] Jafargholi, Amir, Salehi, Mostafa, & Bagheri, Alireza. (2020). Compact dual-band near/far-field dipole antenna/tag. IET Microwaves, Antennas & Propagation, 14(11), 1190-1197.

[11] Nayeri, Payam, Yang, Fan, & Elsherbeni, Atef Z. (2018). Reflectarray Antennas (1st ed., Wiley - IEEE). Somerset: Wiley.

[12] Institution of Engineering Technology, & EuCap 2018. (n.d.). Radiation Pattern Reconfigurable Antenna Design Using Characteristic Modes. 2018 April 19.

[13] Jin, Jianming, & Riley, Douglas J. (2009). Finite Element Analysis of Antennas and Arrays. New York: John Wiley & Sons.

[14] Lemoine, Christophe, Amador, Emmanuel, Besnier, Philippe, Floc'h, Jean-Marie, & Laisne, Alexandre. (2013). Antenna Directivity Measurement in Reverberation Chamber From Rician K-Factor Estimation. IEEE Transactions on Antennas and Propagation, 61(10), 5307-5310.

[15] Zhang, B., Liu, W., & Gou, X. (2017). Compressive sensing based sparse antenna array design for directional modulation. IET Microwaves, Antennas & Propagation, 11(5), 634-641. https://doi.org/10.1049/iet-map.2016.0313.

[16] N. Karmakar. (2020). ECE5122_Design Project Week 10_S2 2020 [PowerPoint slides]. Retrieved from https://lms.monash.edu/mod/folder/view.php?id=7701126.

https://doi.org/10.26549/met.v5i2.6998

SYNERGY PUBLISHING PTE. LTD

Modern Electronic Technology

https://ojs.s-p.sg/index.php/met

Overview of Vehicle AEB

Mingcheng Liu* **Rongwei Shen**

Tianjin University of Technology and Education, Tianjin, 300222, China

ARTICLE INFO

Article history
Received: 24 June 2021
Revised: 30 June 2021
Accepted: 18 October 2021
Published Online: 25 October 2021

Keywords:
Active safety
Vehicle intelligence
Automatic emergency braking

ABSTRACT

With the rapid development of China's economy and the continuous improvement of people's living standards, people pay more attention to the safety of cars. China's car sales and ownership is also rising, but also led to a lot of traffic accidents. With the continuous promotion of intelligent, electric and networked automobiles, Autonomous Emergency Braking system has become the focus of automobile enterprises in the active safety of automobiles. The overall scheme of auto emergency braking includes information acquisition module, control module and execution module. This paper briefly introduces the application status of this field at home and abroad, and discusses the function and implementation method of each module respectively.

1. Introduction

Since the birth of the automobile, the safety problem has been accompanied by around. With the rapid development of the automobile industry, the vehicle safety problem has once again become a problem of great concern to many consumers.

Automatic emergency braking system is a kind of vehicle active safety technology, which is mainly used to reduce vehicle collision accidents. At present, many automobile companies and research institutions in the world are developing automatic emergency braking systems with high reliability [1]. When the vehicle is driving on the normal road, the auto emergency braking system can automatically detect the driving environment. If there is a collision risk in the current driving environment, the vehicle will remind the driver to pay attention through the form of sound and light. When the driver fails to take braking measures, the automatic emergency braking system will automatically take braking measures to avoid the occurrence of traffic accidents.

The National Highway Traffic Safety Administration (NHTSA) and the Insurance Institute for Highway Safety (IIHS) have set a September 1,2022 deadline for automakers to install automatic emergency braking systems in their vehicles.

According to a “report card”published by NHTSA, Tesla has equipped all four of its existing vehicles with automatic safety systems, including forward collision warning, urban emergency braking, high-speed emergency braking, and pedestrian emergency braking. Other U.S. automakers, such as Ford and General Motors, have also started to make good on their commitments, but have yet to equip all their vehicles with automatic

**Corresponding Author:*
Mingcheng Liu,
Tianjin University of Technology and Education, Tianjin, 300222, China;
Email: 131148595@qq.com

 https://doi.org/10.26549/met.v5i2.7361

braking. Ford makes automatic emergency braking a standard feature on its passenger vehicles such as the Edge, Escape, Expedition and Explorer, but makes it optional on vehicles such as the Mustang. Buyers of the F-250 and F-350 will also have the option of automatic braking. Emergency braking is optional on nearly all of GM's Chevrolet vehicles, and the only model that comes standard with forward collision warning, predictive emergency protection and automatic emergency braking is the Equinox. This means that one in 17 Chevrolets will be equipped with automatic emergency braking, but it will still have to install it in all vehicles by September 1, Volkswagen, Audi, Mercedes-Benz and BMW are close to fulfilling that promise. Hyundai, Volvo, Toyota, Subaru and Mazda are also working hard to make good on their promises. The automated emergency system uses on-board sensors, such as radar, cameras or lasers to detect an impending collision and alert the driver, and is capable of braking if the driver does not brake quickly, IHS said. It is estimated that the system could reduce rear-end collisions by 40% [2].

2. Research Status of AEB at Home and Abroad

A prototype of automatic emergency braking first appeared in air vehicles in the1950s. At the end of 1980s, various research institutions and universities began to conduct in-depth research on collision warning and automatic emergency braking system. Since the 21st century, with the rapid development of sensor, computer and other technologies, AEB has attracted the attention of multinational automotive companies. Mercedes-Benz first introduced a collision warning system in 2002, introduced it in the S-class in 2003, and finally introduced its automatic emergency braking system in 2006. Honda introduced a collision warning system with automatic braking on its Inspire model in 2003, which was seen as the beginning of AEB. Subsequently, Volkswagen, Volvo, BMW, Ford Motor and other enterprises have been equipped with this technology on the high-end models. Currently, AEB is available on Audi A6 and QS, Volvo S60 and S80, BMW 5 Series, Ford Taurus and Reveille, and GM Cadillac. AEB has been gradually introduced to China. In China, C-NCAP has prioritized AEB research, which has attracted the attention of joint ventures and self-owned brands to the research, development and application of AEB, and the application models have been extended from high-end to mid-range models [3].

At present, low speed AEB, high speed AEB and AEB pedestrian functions have been achieved mass production, and equipped with medium and high-end models at home and abroad. AEB's main suppliers include Bosch, Continental, Delphi, TRW and other multinational components companies. In addition, Magna, Valeo, Autoliv and other multinational component companies will also form supporting capabilities in the next few years. Domestic enterprises mainly focus on cameras, but there are still no mature products on the market. Hengrun Technology, Hangsheng Electronics, Neusoft Group, Desesiwei, Suzhou Zhihua and other enterprises have successfully developed camera-based FCW, while further AEB is still in the development stage. At the present stage, the cost of AEB for a single sensor scheme is RMB 1,000-2,000. With the continuous technological progress and the gradual expansion of the cost, the annual price reduction rate will be about 3% in the future.

At present, the main models of AEB are medium and high-end models launched by joint ventures such as Changan Ford, Beijing Benz, Dongfeng Nissan and FAW-Volkswagen. The self-owned FAW sedans such as Hongqi H7 and Geely Bo Bei are also used. In recent years, AEB has experienced explosive growth due to the increasing maturity of AEB technology and the acceleration of the equipment process due to the inclusion of AEB in the Euro-NCAP evaluation process [4].

Table 1 shows the AEB assembly of new passenger vehicles in China from 2019 to 2020. From the perspective of various price ranges, the largest proportion of AEB assembly is 100,000-250,000 vehicles. Among them, the main brands are Toyota (Corolla, Leiling), accounting for 38%; Volkswagen (Bora, Lavida), accounting for 13%; 150-200,000 price range, the main brands are Toyota (Camry, RAV4 Rong Rong), accounting for 29%, Volkswagen (Lavida,T-ROC Tanjue), accounting for 20%; The price range is 200,000-250,000, and the main brands are Toyota (Camry, Asialong), accounting for 33%, and Volkswagen (Tanyue), accounting for 23%.

Table 1. AEB assembly in 2019-2020

	2019.1—11	2020.1—11	Year-on-year（%）
AEB assembly apacity (10,000 units)	341.5	521.3	52.6%
AEB Assembly Rate(%)	19.6%	32.3%	64.8%

3. Composition and Principle of AEB

The automatic emergency braking system uses radar (laser radar, millimeter wave radar) to measure the distance with the front vehicle, and then compares this distance with the alarm distance and the safety distance. If the distance between the two vehicles is less than the alarm distance, the alarm promptly will be started. If the

https://doi.org/10.26549/met.v5i2.7361

distance between the two vehicles is less than the safety distance, the vehicle will automatically brake. The system mainly includes three modules: information acquisition module, control module and execution module.

3.1 Information Collection Module

The whole vehicle braking process can be divided into [5]. The driver realizes the occurrence of a dangerous situation and then realizes that emergency measures should be taken. Then the driver raises his right foot and steps on the brake pedal to exert braking force on the vehicle. Finally, the vehicle stops under the action of maximum deceleration, which can be mainly divided into five periods: driver's reaction time (t_1), driver's foot moving time (t_2), braking coordination time (t_3), braking deceleration constant time (t_4). Generally, T1 value is 0.6-1s. Under the ideal condition of ABS, the braking distance of the vehicle can be calculated by the following formula:

$$S = \frac{1}{3.6}\left(t_3 + \frac{t_4}{2}\right)V_1 + \frac{V_1}{254\varphi} \quad (1)$$

Where S represents the braking distance, is the vehicle speed, and is the maximum adhesion coefficient of the road surface.

Vehicle braking distance is related to driving speed, driver reaction time, road adhesion coefficient and brake coordination time, etc. At present, the commonly used ranging methods for vehicles are as follows: ultrasonic ranging, infrared ranging, laser radar ranging, millimeter wave radar ranging, millimeter wave radar low cost, reliable performance, small environmental interference and other advantages, so the vehicle more use millimeter wave radar to measure the vehicle distance.

3.2 Control Model

The control flow chart is shown in Figure 2. In the process of driving, the driver generally has enough time to brake, and the probability of traffic accidents is small. Therefore, the automatic emergency braking system shall first judge the current speed after starting.

Measuring distance is actually measuring the time difference between the transmitting pulse and the echo pulse. Because the electromagnetic wave travels at the speed of light, it can be converted into the precise distance of the target. Because the relative speed between cars is much smaller than the speed of light, it is negligible.If the relative speed between cars is ignored, the distance between two cars can be expressed by Equation (2):

$$R = \frac{1}{2}c\Delta T \quad (2)$$

Where R is the relative distance between the two cars, c is the speed of light, and T is the time interval from transmitting signal to receiving signal. The calculation of the time interval can be done by the timer inside the control processor. Timer starts timing when the signal is transmitted and stops timing when the signal is received, and then reads the time interval numerical substitution Formula (2) of the data register of timer to calculate the vehicle distance. The alarm distance is calculated by Formula (3) and the safety distance is calculated by Formula (1).

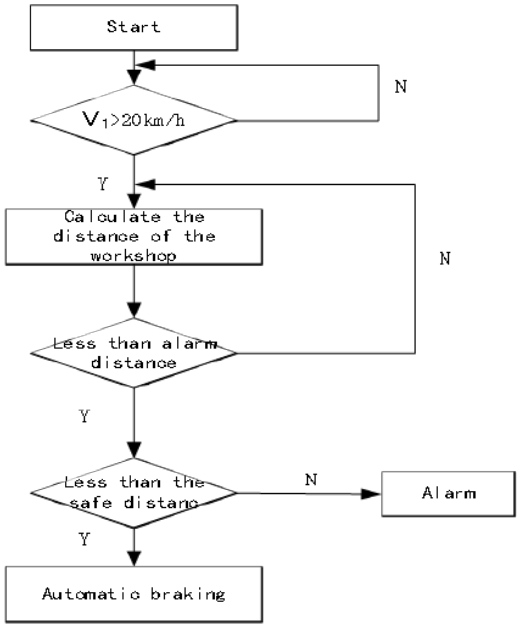

Figure 1. Control flow

$$S = \frac{1}{3.6}\left(t_1 + t_2 + t_3 + \frac{t_4}{2}\right)V_1 + \frac{V_1}{254\varphi} \quad (3)$$

Measured by the speed sensor and set as constant. Adhesion coefficient is selected according to the road conditions. When the system is working, the driver makes the selection according to the actual road conditions at that time and place, and then calculates the distance using Formula (1) and (3). In order to avoid the car in front of the overtaking and vehicles approached, in turn to enter the road cars, pedestrians, when changing lanes or around obstructions caused unnecessary risk, automatic braking and the car when the above situation, must make a turn, so the system control processor made linkage switch, power switch and turn signal switch when calling the turn signal switch. The power switch of the processor is disconnected, and the automatic braking system stops working, so that when overtaking, cornering, changing lanes or going around obstacles, the vehicle in front or its objects will not affect the normal running of the car. When the turn signal switch is turned off, the power switch of the processor is closed and the automatic braking system continues to work [6].

3.3 Perform Module

As shown in Figure 3, in order to simplify the figure, the vacuum main force is omitted. The hydraulic pump

 https://doi.org/10.26549/met.v5i2.7361

2 is driven by the engine through the transmission mechanism and keeps working to produce high pressure. When the vehicle is running at a high speed, the brake fluid oil pressure is required to reach (10-12) MPa to generate the braking torque corresponding to the vehicle speed. Therefore, the brake fluid pressure of the energy storage tank 4 should be kept at 12 MPa, and the relief valve 5 should be set at 14 MPa [7]. When the driver steps on the brake pedal, the high-pressure brake fluid flows into the brake wheel cylinder 8 and pushes the brake block to press the brake disc to realize braking. At this time, the solenoid valve 6, 7 and 11 are closed so that the oil inlet maintains high pressure. When the driver releases the brake pedal, the solenoid valve 6 and 7 are closed, the solenoid valve 11 is opened, and the high-pressure oil flows back to the oil storage room 1 through the oil return road 12. Under the action of the reset spring of the brake wheel cylinder 8, the brake block loosens, thus realizing manual braking.

When the distance of the workshop measured by the system control processor is less than the alarm distance, the output signal of the processor drives the voice chip to give a voice prompt, reminding the driver to take the necessary deceleration operation. When the driver still does not take corresponding measures and the measured workshop distance is less than the safe distance, the output signal of the processor makes the solenoid valve 6 open, the solenoid valve 7, 11 close, the high pressure oil flow of the energy storage tank 4 into the wheel cylinder 8, to achieve automatic braking. At this point, check valve 3 to avoid high pressure oil flow to brake the main cylinder 9 role. If the driver step on the accelerator, the processor is detected after the accelerator pedal position switch signal, and output a high level signal, it has to do with driving solenoid valve 6 signal after and gate, the 7 open the solenoid valve, high pressure oil flow into the single-acting cylinder (10, driving the push rod connected to the clutch mechanism, make the clutch. After the driver releases the accelerator pedal, the solenoid valve 7 closes, until the danger disappears after the solenoid valve 6 closes, the solenoid valve 11 opens, and the high pressure oil in the brake wheel cylinder 8 and single acting cylinder 10 flows back to the oil storage room 1 under the action of the return spring.

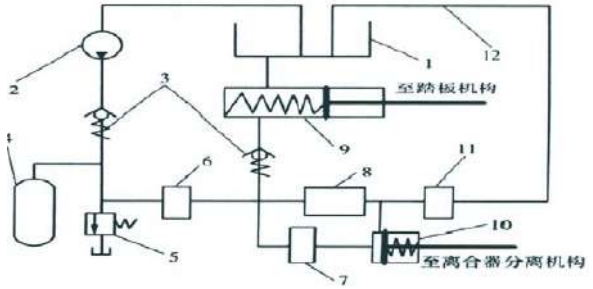

Figure 2. Schematic diagram of automatic actuator
1—Oil chamber; 2—Hydraulic pump; 3—Check valve; 4—Energy storage tank; 5—The overflow valve; 6,7,11—Solenoid valve; 8—Wheel cylinder; 9—Brake master cylinder; 10—The single-acting cylinder; 12—Back to the oil

4. Conclusions

This paper briefly introduces the current situation of AEB at home and abroad, and introduces the three main components and principles of AEB.

In the main information acquisition module, millimeter wave radar is used to measure the vehicle distance, which has strong environmental adaptability, weak environmental interference and suitable detection range. The safety distance and alarm distance of the brake module can be approximated according to the formula. Appropriate improvement of the automatic emergency braking structure can effectively avoid the danger caused by the misoperation.

References

[1] Ministry of Transport.China Transportation Statistics Yearbook.Beijing: People's Communications Press, 2020.

[2] Automatic emergency braking system will become a standard facility in 2022.Driver,2010(6).

[3] Zuo Peiwen.Development status and future trend of automatic emergency braking system.Automotive Industry Research, 2017(2):25~29.

[4] Chen Yirong.Application of auto braking system.Experimental Technology and Management, 2015(11).

[5] Yu Zhisheng.Automotive Theory. Beijing: China Machine Press, 2009.

[6] Stability.Research on a kind of auto braking system. Agricultural Equipment and Vehicle Engineering.2009.

[7] Hu Qinggui.Design of a new auto alarm braking system based on ultrasonic stiffness distance.Automotive Industry Research, 2016.

https://doi.org/10.26549/met.v5i2.7361

SYNERGY PUBLISHING PTE. LTD

Modern Electronic Technology

https://ojs.s-p.sg/index.php/met

Copyright Rules for UGC Platforms: From the Safe Harbor Rule to a Levy Scheme

Weijie Huang*

Law School, Shenzhen University, Shenzhen, Guangdong, 518073, China

ARTICLE INFO

Article history
Received: 26 July 2021
Revised: 31 July 2021
Accepted: 18 October 2021
Published Online: 25 October 2021

Keywords:
Copyright
ISP
UGC platforms
Safe harbor rule
Levy schemes

ABSTRACT

The safe harbor rule was introduced to exempt Internet service providers (ISPs) from liability for copyright infringement committed by ISP users. Nevertheless, the safe harbor rule was crafted for ISPs that provide passive, content-neutral service to distribute copyrighted works. Therefore, the safe harbor rule is difficult to accommodate UGC (user-generated-content) platforms due to their active role in facilitating the distribution and even the creation of copyrighted works. The uncertainty of UGC platforms' liability has led copyright owners to directly target individual UGC creators. In order to unleash the creativity of users without harming the interests of copyright owners, a levy scheme should be introduced. Under the levy scheme, users are allowed to freely use copyrighted works to create UGC for non-commercial purpose. UGC platforms are required to remunerate the copyright owners of the copyrighted works used in the UGC posted on the platforms based on the popularity of the UGC.

1. Introduction

The Internet age features a sharp drop of the cost to distribute and share copyrighted works, followed by large-scale copyright infringement. Due to the large number of actual infringers, i.e., internet users, and the high cost of launching lawsuits against individual users, copyright owners have tended to shift their target to distribution intermediaries with deep pockets, i.e., internet service providers (ISPs) [1]. Nevertheless, with the ambition to promote information technology to achieve competitive advantages in the global market, legislators have decided to side with ISPs. The two most representative copyright laws in the early Internet age, the Digital Millennium Copyright Act (DMCA) enacted by the US in 1998 and the Electronic Commerce Directive (eCommerce Directive) passed in the EU in 2000, were both characterized by such national strategy. The most obvious manifestation of such strategy is called the safe harbor doctrine, a rule that exempts certain Internet service providers (ISPs) from liability for copyright infringements committed by ISP users.

The ISPs shielded by the safe harbor rule do not facilitate or profit from the distribution of copyrighted works, but merely transmit, cache, store and locate copyrighted works as passive conduits [2]. In other words, these ISPs have played a passive role in distributing copyrighted content. The safe harbor rule has indeed encouraged the development of information technology, as the legislators wished. However, the breathing

**Corresponding Author:*
Weijie Huang,
Law School, Shenzhen University, Shenzhen, Guangdong, 518073, China;
Email: gdsthwj106@163.com

 https://doi.org/10.26549/met.v5i2.7711

space provided by the robust safe harbor doctrine has engendered new online intermediaries that the legislators did not anticipate. These online platforms have played a much more active role in distributing or even producing copyrighted content, and thus it is difficult to be accommodated by the safe harbor rule. One example is UGC (user-generated-content) platforms, such as YouTube, Tiktok and Wechat.

This article articulates the need for a new copyright rule governing UGC platforms. By analyzing the origin and purpose of the safe harbor doctrine, Section 2 explains the reason for crafting it in the Web 1.0 era. Section 3 describes how the safe harbor doctrine cannot be adapted to UGC platforms, and the inefficiency and injustice of imposing liability on individual users. The article concludes with a call for a levy scheme for UGC platforms to balance the interests of users, copyright owners and online platforms.

2. The Origin and Purpose of the Safe Harbor Rule

The safe harbor doctrine is generally considered to be proposed to develop domestic Internet technologies to maintain a national competitive edge in the 21st century. As the U.S. congressional report noted, ISPs' liability for third-party infringement required clarification for fear that ISPs 'may hesitate to make the necessary investment in the expansion of the speed and capacity of the Internet [3]. This article argues that a more essential but often overlooked reason for introducing the safe harbor doctrine is that ISPs played a much more passive role in distributing copyrighted works than previous distributors had.

In the pre-Internet age, some distributors, such as broadcasters and cable television operators, directly used the copyrighted works. In this article, they are referred to as user-distributors. User-distributors directly subject to the proprietary copyright rules as they are the users. Some distributors, such as the video cassette recorders and digital audio recorders, did not directly use the copyrighted works, but provided devices to facilitate the use of the works and profited from users' use of copyrighted work. In this article, this category of distributors is referred to as facilitator-distributors. They are usually subject to levy schemes under which facilitator-distributors need to remunerate copyright owners while users can freely use copyrighted material for non-commercial purpose [4].

ISPs under the safe harbor doctrine have played an even more passive role than facilitator-distributors. The safe harbor doctrine only applies to ISPs that perform the following functions: (i) transitory digital network communications, (ii) system caching, (iii) storage of information at the direction of the users and (iv) information location tools [5]. These ISPs do not supply tools to facilitate users' distribution of copyrighted works, but merely provide technical, passive and content-neutral services for copyrighted works generated by third parties. ISPs' passiveness and neutrality are the prerequisites for them to enter the safe harbor.

3. Inadaptability of the Safe Harbor Rule to UGC Platforms

UGC (user-generated-content), which refers to content created or re-created by amateurs online, has attracted the attention of copyright owners as most UGC have used and adapted others' copyrighted material. UGC creators who use others' copyrighted material to create UGC may constitute infringement, but UGC platforms seem to be sheltered by the safe harbor doctrine as they seem to meet the category of "storage of information at the direction of the users". Nevertheless, case law has shown the hesitance of courts to place UGC platforms into the safe harbor [6].

This article finds that the uncertainty of the applicability of the safe harbor doctrine to UGC platforms is rooted in the UGC platforms' active and volitional role in the management and even promotion of content. UGC is characterized by the decentralization of content production. In the pre-Internet era, content production engendered enormous cost and could only be undertaken by professional producers such as publishing houses. Producers were motivated to select a few high-quality creations to recoup investment. In this sense, producers acted as a filter of content. In the UGC age, every user can make their creation available to the public regardless of the quality of the content. Decentralized and abundant creations call for a centralized intermediary to manage and organize the content. UGC platforms have emerged to take on this role by, for example, categorizing unordered UGC according to individualized preferences, guiding content production by cooperating with MCNs (Multi-Channel Networks), and enhancing the appeal of UGC by promoting the interaction between UGC creators and users [7].

Furthermore, UGC platforms can draw direct financial benefits such as advertisement from popular UGC. For example, YouTube was valued at US$170 billion in 2020 with more than 500 hours of videos uploaded per minute [8]. Wechat's revenue reached RMB 108.2 billion in 2020, an increase of nearly 20% compared to 2019 [9]. In a word, UGC platforms have gone far beyond ISPs' passive, content-neutral and profit-free role assumed by

https://doi.org/10.26549/met.v5i2.7711

the legislators of the safe harbor rule, but have played a role more like facilitator-distributor.

The uncertainty of whether UGC platforms should be liable for copyright infringement, in turn, has encouraged the cooperation of UGC platforms and copyright owners against users [10]. By requiring UGC platforms to disclose information of the infringing users, copyright owners can directly launch lawsuits against the users. Although most of the creation and the use of UGC is non-commercial, copyright owners claimed that the wide distribution of UGC would unreasonably prejudice their legitimate interests and seize their opportunity to make derivative works [11]. Nevertheless, imposing liability on individual users for their non-commercial use of copyrighted works is unfair and would hamper users' creativity and privacy. Furthermore, it would encourage violations of the law. Given the countless number of individual users and the cost of litigation, targeted users would be randomly chosen. If a user knows that there is only a small probability of being sued and that s/he cannot control such probability, s/he would have no incentive to obey the law [12]. Furthermore, copyright owners would have difficulties in enforcing their copyright due to the high cost of litigation. The uncertainty of the safe harbor rule would also prevent UGC platforms from making technological innovation to promote the creation and management of UGC. It is urgent to craft a new copyright rule addressing the copyright infringement committed by platform users.

4. A Levy Scheme for UGC Platforms

This article proposes a levy scheme imposed on UGC platforms. The history of copyright law indicates that distributors' liability is equivalent to the role they play in the distribution of works. User-distributors are subject to proprietary rules under the exclusive copyright regime as they directly use copyrighted works. Facilitator-distributors are subject to levy schemes since they do not use but facilitate users to use of copyrighted works, and gain profit from users' use. ISPs that do not facilitate the use of copyrighted works, but merely provide technical, passive and content-neutral services to distribute copyrighted works are therefore sheltered by the safe harbor rule. UGC platforms do not directly use copyrighted works, but promote the dissemination and even the creation of copyrighted works and benefit from it. Therefore, UGC platforms have assumed the role of facilitator-distributors rather than the role of the passive, content-neutral ISPs. Accordingly, UGC platforms should be regulated by a levy scheme.

The levy scheme is not only faithful to earlier copyright history, but also responds well to actual needs of spurring creativity brought by the decentralization of content production and distribution. Users are free to use copyrighted material to create UGC for non-commercial purposes. UGC platforms should make reasonable payment, i.e., levies, to copyright owners of the copyrighted works used in the UGC posted on the platforms according to the popularity of the UGC. In this way, users can acquire breathing space for private use and re-creation. Copyright owners can gain fair remuneration of their works. UGC platforms can save the cost of monitoring and avoid legal risks.

Funding

This work was supported by Guangdong Planning Office of Philosophy and Social Sciences 2020 (project no. GD20YFX05).

References

[1] *See* Playboy Enterprises, Inc. v. Frena, 839 F. Supp. 1552, 1568 (M.D. Fla. 1993); Religious Technology Center v. Netcom On-Line Communication Services, Inc., 907 F. Supp. 1361, 1370 (N.D. Cal. 1995); Spindler G, 2020. Copyright Law and Internet Intermediaries Liability. In: EU Internet Law in the Digital Era, Synodinou T et al. (eds.), Springer, 3-25.

[2] 17 U.S. Code § 512 (a), (b), (c) and (d). Driscoll M, 2007. Will YouTube sail into the DMCA's safe harbor or sink for internet piracy? The John Marshall Review of Intellectual Property Law, 2007 (6): 555.

[3] S. Rept.105-190, 1998: 8.

[4] Kretschmer M, 2012. Private Copying and Fair Compensation: An Empirical Study of Copyright Levies in Europe. London: Intellectual Property Office, 10.

[5] 17 U.S. Code § 512 (a), (b), (c) and (d).

[6] *See* different judicial opinions in CoStar Group vs. LoopNet (373 F.3d 544, 556 (4th Cir. 2004)), Capitol Records v. Vimeo (826 F.3d 78, 96 (2d Cir. 2016)), and BWP Media v. Clarity(820 F.3d 1175, 1178 (10th Cir. 2016)).

[7] Senftleben M, 2020. Institutionalized algorithmic enforcement-The pros and cons of the EU approach to UGC platform liability, Florida International University Law Review, 14(2): 312-313.

[8] Mohsin M. 10 Youtube stats every marketer should know in 2021. Retrieved July 25, 2021, from https://www.oberlo.com/blog/youtube-statistics.

[9] Iqbal M. Wechat revenue and usage statistics (2021). Retrieved July 25, 2021, from https://www.businessofapps.com/data/wechat-statistics/.

[10] Li Y & Huang W, 2019. Taking users' rights seriously: proposed UGC solutions for spurring creativity in

 https://doi.org/10.26549/met.v5i2.7711

the Internet age. Queen Mary Journal of Intellectual Property, 9(1): 72.

[11] Presseller S, 2017. Copyright infringement via social media live streaming shortcomings of the digital millennium copyright act. Arizona State University Sports and Entertainment Law Journal, 2017 (7): 376.

[12] Lichtman D & Landes W, 2002. Indirect liability for copyright infringement: An economic perspective. Harvard Journal of Law & Technology, 2002(16): 409.

https://doi.org/10.26549/met.v5i2.7711

SYNERGY PUBLISHING PTE. LTD

Modern Electronic Technology

https://ojs.s-p.sg/index.php/met

A Review of Traffic Conflict Avoidance Methods at Intersection Using Vehicle-Infrastructure Cooperation System

Danping Wang*

School of Automobile and Transportation, Tianjin University of Technology and Education, Tianjin, 300222, China

ARTICLE INFO

Article history
Received: 20 September 2021
Revised: 27 September 2021
Accepted: 18 October 2021
Published Online: 25 October 2021

Keywords:
Traffic conflict avoidance algorithm
Intersection
Vehicle-Infrastructure Cooperation System (VICS)

ABSTRACT

Road intersections are important nodes for the convergence, turning, and diversion of traffic flows in the urban road network, but at the same time, due to the large traffic volume and conflict points at the intersection, it has become a traffic congestion and accident-prone area, which seriously affects road traffic safety and vehicle traffic efficiency. Therefore, it is of great significance to study the collaborative control strategy of urban intersections. This paper analyzes and summarizes the methods of intersection cooperative control based on intelligent connected vehicles in recent years, and looks forward to the future development trend and prospects of the combination of intersection cooperative control and Vehicle-Infrastructure Cooperation System.

1. Introduction

Intersection is an important road traffic node in the city, which is a link between roads in different directions. According to statistical data, about 36% of traffic accidents in the United States are related to intersections, and about 35% of traffic accidents resulting in injuries or deaths are related to intersections [1,2]; Traffic fatalities and injuries at intersections account for more than 20% of total accidents in Europe [3]; Japan has 42% of traffic accidents at intersections [4]. In the more densely populated urban roads, 80% of the traffic delays are related to road intersections. The efficiency of vehicle movement at road intersections is only 50% of the efficiency of movement on other road sections [5]. The determination of intersection access priority, between vehicles these are the main reasons for the frequency of traffic accidents at intersections. With the application of computer technology, control technology, electronic sensing technology and other research and development integration in the intelligent transportation, how to control the intersection operation with the consideration of traffic delay, energy consumption, has also become one of the hot spots of many scholars research. By effectively linking information on vehicle operations, drivers, and the road network environment through communication networks, establish a close coupling of cooperative control to achieve an information and intelligent traffic control system, Reduces vehicle delays and traffic accidents by resolving conflicts over intersection space-time resources.

**Corresponding Author:*
Danping Wang,
School of Automobile and Transportation, Tianjin University of Technology and Education, Tianjin, 300222, China;
Email: 1933835537@qq.com

 https://doi.org/10.26549/met.v5i2.8491

2. Collaborative Traffic Control System at Intersections Using VICS

Traditional intersection control methods are mainly divided into signalized and unsignalized control. Intersection control with signals generally calculates the estimated time of green light for an intersection based on the car travel delay equation, and cannot adjust the signal timing according to the current traffic flow, weather conditions and road information, which has certain limitations. Traffic control methods with signalization include. (1) Single-point timing multi-phase signal coordination control, i.e., calling a preset scheme by clock to reduce traffic conflicts, in conjunction with early break and late start when necessary. (2) Vehicle sensing real-time adaptive coordination control, i.e., by adjusting the period, green letter ratio, and increasing the effective green light time, etc., in accordance with the arrival of traffic flow. (3) User priority cable-free arterial coordination control, which refers to "green wave control" used on arterials to prioritize traffic flow on arterials by coordinating cycle and phase differences and taking care of pedestrians, buses, special vehicles, etc. (4) Real-time adaptive area control refers to the optimization of efficiency indicators, traffic flow simulation and other advanced means to ultimately achieve the purpose of balanced regional traffic flow. Han Yilei et al [6] conducted statistics on traffic volume and signal timing at intersections in the morning and evening peak hours. Optimize the design of the intersection capacity in terms of lane function division and signal timing, etc. based on VISSIM, the solution design was verified to reduce the average delay of intersection vehicles by 55.77%. The intersection traffic flow dynamic control method was studied by Liang Zijun et al [7]. Viewing traffic flows as independent control units and proposing a variety of cooperative control logics. It is also verified that the method can reduce the phenomenon of vehicle congestion at intersections.

Unsignalized intersections are prone to traffic accidents due to the control method of non-right-of-way assignment and signal-guided management. General through the unsignalized intersection is the vehicle approaching the intersection area to observe the intersection conditions in advance, to determine whether the vehicle through or slow down and stop. At present, the control mode of signal-less intersection is mainly divided into vehicle-vehicle cooperative control mode and central control station control mode. Vehicle-vehicle cooperative control is to be informed of the location, speed and road conditions of the surrounding vehicles through sensors. Regulating the speed and trajectory of self-vehicles can solve the problem of conflicting spatial and temporal resources that exist when vehicles pass through intersections. The method can be effectively implemented in road conditions with fewer vehicles, but when the intersection traffic volume is high and the road conditions are complex, it is impossible to macro-regulate the intersection vehicles. When the central control station control mode is used, the vehicle communicates mainly with the roadside intelligent devices. A large amount of information interaction between different vehicles is avoided, thus reducing the system requirements for wireless communication networks to some extent.

2.1 Framework of VICS

VICS-based intersection control is a real-time data collection of raw sensory data such as images and video point clouds in the current coverage area through sensory devices such as cameras and millimeter wave radar. Send the collected real-time data to the road test calculation control unit for real-time processing. Obtaining participant status information, road condition information, traffic flow information, weather information, etc. of the road traffic environment. send the processed information to the vehicle subsystem or other road subsystem via the road test unit in real time; When a centralized control of the vehicle is required, Intelligent roadside computing control unit for autonomous driving, which can specify control strategies based on the prevailing traffic conditions and the individual conditions of the vehicle. The decision planning strategy and control data are sent down to the vehicle subsystem, and the vehicle-side computing control unit processes the raw sensing data from the on-board sensing devices in real time. Obtain information on the status of traffic participants in the road traffic environment, etc. The processed information will be notified in real time to the vehicle subsystem or road subsystem via the on-board unit. Generate the vehicle's driving strategy in real time and send the driving strategy to the autonomous vehicle's in-line control system The in-line control system controls the vehicle via the vehicle bus, in-vehicle Ethernet and other links. including control of the vehicle's braking system, steering system, transmission system, body control, etc. It is also able to control vehicle acceleration, deceleration, steering, lights, double flashing, etc. The roadside traffic control facility regulates traffic conditions through traffic signals, dynamic speed limits and other strategies based on data processed in real time from current data. Resolve congestion caused by traffic conflicts at intersections. The VICS-based intersection control system is shown in Figure 1:

https://doi.org/10.26549/met.v5i2.8491

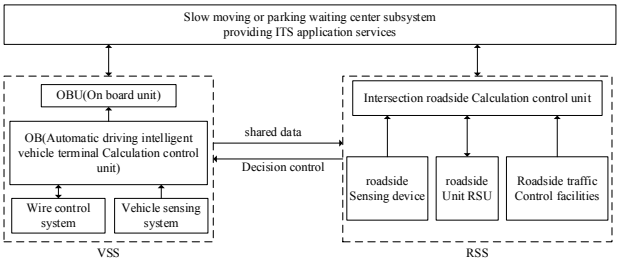

Figure 1. The intersection control system based on vehicle-road cooperation

2.2 Traffic Applications Using CIVS

Comparison of traffic conflict avoidance models S. Jin et al. [8] based on cooperative control system, for intersection without signal control proposed the use of improved hybrid frog-hopping algorithm to develop an optimal strategy to avoid collisions, wireless communication technology can obtain information between vehicles and vehicles and between vehicles and control center, which improves the stopping delay time, travel time, and vehicle traffic efficiency. Wenjuan E [9] proposed a vehicle conflict monitoring and elimination strategy based on vehicle-road cooperative technology to obtain vehicle perimeter information, set the priority level of passage for vehicles approaching at the intersection, and establish an intersection passage rule base for the problem of vehicle conflicts at unsignalized intersections. Zhou Jianshan et al. [10] studied the optimization of signal control at single-point signal intersections and used neural computation principles and fuzzy decision-making techniques in signal optimization control strategies to establish optimal signal timing schemes considering the diversity of traffic flow patterns, in order to online traffic flow OD estimation, a traffic OD matrix estimation model based on the principle of great entropy, a SOM neural network model, and a Takagi-Sugeno-Kang fuzzy decision system for effective identification and optimal control of traffic flow patterns at single-point signal intersections. According to the local development plan (such as industrial areas, residential areas, scenic spots, etc.) the time of day or each week or quarter population flow presents certain regular characteristics, and the signal timing scheme is designed according to the law of data mastered by the survey, but this law needs to consume long time and large labor cost, and with the economic development population flow will also change, not with real-time, and less adaptable range [11-13]. Dresner K et al. [14] established a multi-agent intersection coordination control center based on a vehicle-road cooperative system, which sends the operational status to the control center when the vehicle reaches the control range and the control center coordinates to guide the vehicle speed based on the current traffic flow information of the road.

Traditional signalized intersections can avoid vehicle conflicts to a certain extent, but they are prone to traffic congestion because they cannot be adjusted according to traffic flow and road conditions. The unsignalized intersection control method can be effectively executed for the road conditions with low traffic flow, but it is less effective for the complex road conditions with high traffic flow and cannot play a macro control role. With the continuous development of smart networked vehicle technology, the centralized processing of vehicle information can also meet the requirement of real-time. Makes it possible to control the behavior of vehicles at unsignalized intersections using Smart Grid technology. For cooperative vehicle-road control systems the efficiency of the control algorithm generation directly affects the safety and efficiency of road traffic. Therefore, effective conflict avoidance and traffic efficiency improvement are of great importance to the research of vehicle-road cooperative control.

3. Comparison of Traffic Conflict Avoidance Models

Currently, there have been many studies on vehicle conflict coordination control algorithms at intersections. With the development of vehicle-road cooperative intelligent networked vehicles, intersection passage no longer relies solely on signal control, and the fundamental problem of conflict elimination is still how to coordinate control between vehicles. At present, there are mainly acceptable gap model, control model based on dynamic game theory, conflict collision avoidance decision model based on dominance and conflict table algorithm based on resource lock.

3.1 Acceptable Gap Model

In 1968, Drew [15] proposed an acceptable gap model for the interpolation gap of vehicle operation at unsignalized intersections after analysis of the system. Vehicles that need to merge into the target lane at the intersection should slow down in advance to observe the traffic conditions and whether there are conditions (interpolable gap), and when the actual gap is greater than the acceptable critical gap in the driver's mind, they can wait for the opportunity to adjust the speed through the intersection, otherwise slow down or stop and wait for the right time.

 https://doi.org/10.26549/met.v5i2.8491

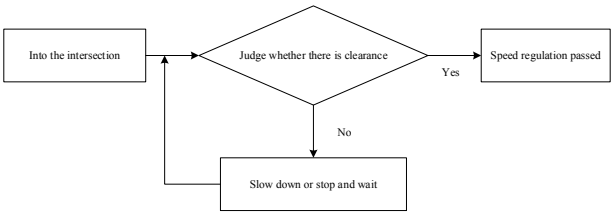

Figure 2. Driving mode through intersection based on acceptable gap model

A critical gap calculation method based on roundabouts considering driver behavior, vehicle travel characteristics and roundabout entrance geometry characteristics was proposed by Jia Hongfei et al. [16] The capacity simulation error of 4.2% was calculated by investigating the weekday evening peak data, which is a significant reduction compared with the capacity simulation error of 7.7% by the Raff method, 15% by the great likelihood method, and 18.6% by the Ashworth method, but the influence of pedestrians and non-motorized vehicles was ignored in the data investigation, which still has a certain error compared with the real data. However, the effect of pedestrians and non-motorized vehicles is ignored in the data investigation, and there is still some error with the real data. Hailong Gao et al. [17] established a mathematical model for analyzing and calculating critical clearance considering driver and vehicle characteristics to verify its feasibility. Different drivers generate different pressures through different intersections, and the intersection road conditions are complex, and the critical clearance can vary.

3.2 A Conflict Avoidance Decision Model Based on Preemptive Level

Based on the dominant model refers to the vehicle in the conflict point of the dominant position and the psychological factors of the driver to determine the priority of the vehicle in the conflict point of passage. The driver observes in advance whether there is a conflict point between his own vehicle and the surrounding vehicles in the future running trajectory, if there is no conflict point can pass normally, if there is a conflict point according to the actual situation of the corresponding conflict avoidance decision. Amundsen et al. [18] in 1977 studied intersections to give a suitable definition of traffic conflict: a traffic conflict is a conflict of resources in time and space for operating vehicles, and a collision occurs if this resource conflict problem cannot be coordinated in advance. Xiao Yongjian et al. [19] considered the influence of driver psychological factors and established a subject-object virtual trajectory field where the vehicle has passed the body length of the conflict point to calculate the dominance assessment in the conflict, introducing a critical dominance characterizing the driver's decision threshold, and the field collection parameters were calibrated to verify that the method obeys a normal distribution $N(0,0.2^2)$.

3.3 Control Model Based on Game Theory

The game can be divided into a static game and a dynamic game according to the state, and the participants of the static game only take action once at the same time. In many conflict resolution models, the study of the driver's decision to perform the conflict belongs to one decision, ignoring the analysis of the mutual influence between different drivers' behavioral decisions in the process of intersection. Repeated game is a special kind of discrete dynamic game, assuming that the set of participants at the intersection conflict point is A= {A1, A2,A3}, as shown in Figure 3 below:

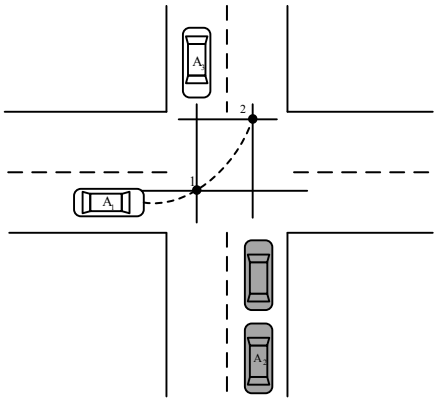

Figure 3. Schematic diagram of vehicle insertion at unsignalized intersection

The multiple times game in the process of car insertion uses game tree to represent the acceleration and deceleration and decision time characteristics, in which different driver behaviors have a great impact on the outcome of the game. Liu et al. [20] analyzed the driver behavioral decision at a smaller spatial scale, established a model of driver intersection intersection behavior without light control based on dynamic repeated games, classified drivers into cautious and risky free combination types, analyzed the Nash equilibrium and driver behavioral decision in the intersection game process, and proved the reasonableness of the model. The Nash equilibrium and drivers' behavioral decisions in the intersection game are analyzed, and the rationality of the model is proved. However, multiple gaming can sometimes have an impact on vehicle travel, and the effectiveness of this algorithm has yet to be verified in the case of more vehicles at intersections. Jingxian Li [21] analyzed the interfering nature of pedestrians on straight ahead and left-turning

https://doi.org/10.26549/met.v5i2.8491

vehicles, according to the optimal control strategy and rule making taken when vehicles travel in different directions on the road with pedestrians crossing the road for gaming, from the practical point of view non-motorized vehicles are also one of the very important interfering factors. Liu Na [22] established a dynamic game model of straight and left turn when considering the influence of driver personality factors on straight and left turn conflicts, whether this method is applicable to other conflict point elimination at intersections remains to be studied in depth.

4. Conclusions and Discussions

The intersection cooperative control method has been studied and summarized, and it is found that the intersection cooperative control only relies on the traffic signal and the information interaction between vehicles to solve the intersection conflict problem, which has certain limitations. If these methods are combined with the vehicle-road cooperative technology, the information obtained by advanced road measurement equipment and vehicle-mounted units can be used to provide a reference basis for intersection conflict resolution, and if each intersection is also controlled in cooperation with each other, the capacity of vehicles on the road will be greatly improved.

Funding

Tinajin Research Tnnovation Project for Postgraduate Students: Research on multi-sensor fusion vehicle detection algorithm in complex weather conditions(2020YJSS086).

References

[1] E.Commission. Traffic Safety Basic Facts on Seasonality[R]. Technical Report, 2016.

[2] S.Huang, A.W.Sadek and Y.Zhao. Assessing the mobility and environmental benefits of reservation-based intelligent intersections using an integrated simulator[J]. IEEE Transactions on Intelligent Transportation Systems,2012, 13(3):1201-1214.

[3] European Road Safety Observatory. Traffic Safety Basic Facts 2006 Junctions[EB/OL]. Safety Net, Project co-financed by the European Commission, 2007, 4.

[4] Xie Boyuan. Vehicle Cooperative Control Basd on Information Exchange and Motion Coupling [D]. Beijing: Tsinghua University,2014.

[5] SUN Liyun. Research on Urban Road Intersections-accident Prediction Model and Algorithm [D]. Beijing Jiaotong University,2011.

[6] HAN Yilei, HAN Yin, HU Rong. Optimization Design of Intersection Traffic Organization Based on VISSIM Simulation [J]. Logistics Sci-Tech,2021,44(09):83-86.

[7] LIANG Zijun,ZHANG Weihua,YANG Wei, et al. Research on dynamic control method of traffic streams at intersection based on time space resouree optimization [J]. Journal of Hefei University of Technology (NATURAL SCIENCE),2020,43(09):1240-1249.

[8] JIN Li-sheng,ZHENG Yi,GAO Lin-lin, et al. Cooperative vehicle intersection control algorithm for intelligent vehicles [J]. Journal of Chang'an University (Natural Science Edition),2015,35(S1):7-11.

[9] E Wenjuan. Reasearch on Vehicle Conflict Detection and Resolution Algorithm at Unsignalized Intersection [D].JilinUniversity,2012.

[10] Jianshan Zhou,Daxin Tian,Xu Han et al. A Self-adaptive Optimal Control Approach for Urban Isolated Signalized Intersection Based on VII [A]. China Intelligent Transportation Association. The 7th China Intelligent Transportation Conference Excellent Paper Collection - Intelligent Transportation Technology [C]. China Intelligent Transportation Association: China Intelligent Transportation Association,2012:12.

[11] CHEN Yudong, ZHANG Yi, HU Jianming et al. Pattern Discovering of Regional Traffic Status with Self-Organizing Maps[J]. In Proceedings of the IEEE ITSC, 2006, MC7.5: 647-652.

[12] Wong Y.K, Woon W.L. Improving traffic signal control system using demining[J]. In Proceedings of the MMU international symposium of information and communication technologies, 2006.

[13] Wong Y.K, Woon W.L. An iterative approach to enhance traffic signal optimization[J]. Expert Systems with Application, 2008, 34(4):2885-2890.

[14] Dresner K, Stone P.A multiagent approach to autonomous intersection management[J]. Joournal of Artificisl Intelligent Research 2008,31(1),591-656.

[15] Qu Zhaowei,Jin Yong,Chen Yongheng,et al.Planning methods and effect analysis of advance right-turn[J]. Journal of Traffic and Transportation Engineering,2008,8(2):106-109,115.

[16] JIA Hongfei,LI Bolin.Calculation of Traffic Capacity at Signalized Roundabouts Based on Gap Acceptance Theory[J].Journal of Transport Information and Safety,2018,36(03):64-71.

[17] GAO Hailong,WANG Wei,CHANG Yulin, et al. A mathematical model for critical gap of unsignalized intersections[J]. China Journal of Highway and Transport,2001(02):80-82.

[18] CHIN H C,QUEK S T. Measurement of traffic conflicts[J].Safety Science,1997,26(3):169-185.

[19] XIAO Yongjian,YANG Jianguo,WANG Zhaoan.

 https://doi.org/10.26549/met.v5i2.8491

Driver's conflict avoidance decision model based on preemptive level[J]. Journal of Traffic and Transportation Engineering,2009,9(05):116-120.

[20] LIU Xiao-ming, WANG Xiu-ying Vehicle-cross Action Model in Intersection Without Traffic Light Based on Reduplicate Game [J]. China Journal of Highway and Transport,2011,24(04):94-100.

[21] Li Jingxian Traffic Signal Optimization Based on game models of the Interference of Turning Traffic in the Intersection [D]. Chang'an University,2018.

[22] Liu Na. Research on Conflict Model of Straight and Left Turning Vehicles Based on Game [D]. Xi'an University of Architecture and Technology,2019.

https://doi.org/10.26549/met.v5i2.8491

SYNERGY PUBLISHING PTE. LTD

Modern Electronic Technology

https://ojs.s-p.sg/index.php/met

Design of a Submarine Pipeline Inspection Robot System Based on CT Technology

Xu Dong[1*] Wenyu Zhang[1] Yishun Li[1] Wei Liu[2] Li Yang[3]

1. Beijing Research institute of Mechanical & Electrical Technology, Beijing, 100074, China
2. Liaoning Vocational Technical College of Modern Service, Shenyang, Liaoning, 110000, China
3. Beijing Oil and Gas Transportation Branch of National Pipe Network Group North Pipeline Co., Ltd. Beijing, 102488, China

ARTICLE INFO

Article history
Received: 20 September 2021
Revised: 27 September 2021
Accepted: 18 October 2021
Published Online: 25 October 2021

Keywords:
Submarine oil and gas pipeline
ROV robot
CT technology
Non-invasive inspection

ABSTRACT

With the rapid development of submarine oil and gas, the security issues of submarine oil and gas pipeline become increasingly prominent, and regular inspection of submarine pipeline is particularly important. Therefore, a submarine pipeline inspection robot system based on CT technology to solve the problems such as low traditional manual inspection efficiency, high labor cost, low security and backward inspection methods. Based on the platform of ROV robot, carrying CT scanner as an external detection device, the system is used for non-invasive inspection of submarine pipeline, which is safe and harmless, with good economy, high mobility, and strong environmental adaptability. Compared with traditional technology, CT scanner's external inspection technology used in the system avoids the damage to the external protective layer of the pipeline in the measurement of pipeline wall thickness. Meantime, it can provide the tomography of the pipe wall and the composition of the sediment material on the inside wall, which fills the gap in this technical field in China. According to the test, the robot has the characteristics of stable adsorption, flexible movement, and clear pipeline CT scanning image, and can realize the intelligent inspection of submarine pipeline.

1. Introduction

In recent decades, with the rapid development of offshore oil and natural gas by countries all over the world, submarine oil and gas pipeline has become the safest, fastest, most reliable and most economical method to continuously transport a large quantity of oil and natural gas. It plays an important role in the transportation of offshore oil and natural gas, considered as the lifeline of offshore oil and gas transportation engineering. Since the first submarine oil and gas pipeline was built by Brown & Root (an American ocean engineering corporation) in the Gulf of Mexico in 1954, a huge submarine oil and gas pipeline network has been formed in various sea areas worldwide [1]. In 1985, the first submarine oil pipeline was laid in Chengbei oilfield, Bohai Sea [2]. Up to now, the total length of submarine pipelines laid in different sea areas in China has exceeded 6,000 km.

Due to complex marine environment, oil and gas transmission pipeline is affected by natural factors such as geological changes, medium corrosion and ocean current impact for a long time, or damaged by artificial factors such as sand mining and anchor, so the pipeline is prone to corrosion, cracks and other problems [3-5]. If these

**Corresponding Author:*
Xu Dong,
Beijing Research institute of Mechanical & Electrical Technology, Beijing, 100074, China;
Email: dongxu53@163.com

 https://doi.org/10.26549/met.v5i2.8529

problems cannot be found in time, oil and gas leakage accidents caused by the damage to oil and gas pipelines will directly lead to shutdown of oil and gas fields, and even explosion due to leakage of crude oil or natural gas, resulting in heavy casualties and huge economic losses, and seriously destroying the surrounding ecological environment [6,7]. In 2007, the crude oil pipeline in Weizhou Island, South China Sea leaked due to corrosion, resulting in the shutdown of Weizhou oilfield for nearly 200 days [8]. In 2011, due to illegal operation of sand mining ship near CNOOC (Hengqin, Zhuhai) natural gas, CNOOC natural gas pipeline was mechanically damaged and broken [9], resulting in a serious leakage accident. In recent years, as submarine pipeline is continuously built and submarine pipeline accidents gradually increase, the safety protection of submarine pipeline has become increasingly important, and the regular inspection of submarine pipeline has become an increasing concern. It is an important way to ensure the normal and safe operation of submarine pipeline to regularly inspect, accurately locate and find the damage and failure of pipelines.

The traditional method of divers inspecting pipeline by handheld device has the characteristics of low efficiency, high labor cost and low safety. When the development of China's marine oil and gas resources gradually extends from shallow water area (Bohai Sea area) to deep water area (Yellow Sea and South China Sea areas), it is much more difficult to lay, install, inspect and maintain oil and gas facilities and to work underwater for divers, and the risk of operation by personnel become higher [10]. Furthermore, the traditional inspection methods are no longer suitable for the current inspection scenario, so it is very important to design and produce an intelligent robot that can replace divers for underwater inspection.

At present, the inspection method of submarine oil pipeline is mainly internal inspection, using technologies such as magnetic flux leakage [11,12], ultrasonic [13], electromagnetic wave [14] and eddy current [15,16], but these technologies can only be used on land, that is, internal inspection cannot be conducted after the pipeline is laid underwater. Therefore, it is urgently needed to solve the technical problem of external inspection of pipeline.

Based on the necessity of submarine pipeline inspection and our previous research on submarine robot and external pipeline inspection technology, a non-invasive submarine pipeline inspection robot based on CT technology is designed. Through the overwater control system, we remotely monitor and control the ROV robot platform, carry and place the CT scanner to the submarine pipeline, complete the independent inspection of the submarine pipeline, and feed back the relevant data, images and processing results in real time. Compared with the traditional inspection technology, CT scanner avoids the damage to the external protective layer of the pipeline in the measurement of pipeline wall thickness. Meantime, it can provide the CT scan of the pipeline wall and the composition of sediment on the inside wall. This is a breakthrough in domestic non-invasive inspection technology.

2. Design of Submarine Pipeline Inspection Robot System

2.1 System Introduction

The submarine pipeline inspection robot system () is mainly composed of submarine pipeline inspection robot platform, platform load (CT scanner, Tanker, etc.) and overwater control system. The platform load is carried by the submarine pipeline inspection robot platform. The signal interaction and energy supply between the overwater control system and the underwater robot are realized through wire transmission.

2.2 Design of Control System for Submarine Pipeline Inspection Robot

The function of the control system is to sense the external information through the sensor and analyze, judge and process the information, send control commands through the output interface, coordinate the work of each subsystem, control the rotational speed and direction of the thruster, and display the status of each system. The control system can precisely control the underwater robot in water, including fixed depth navigation, fixed speed navigation, directional navigation, positioning hovering, and crawler traveling under the interference of complex ocean current.

2.2.1 Composition of Control System

The control system of submarine pipeline inspection robot (Figure 2) is composed of computer, RS485 bus, thruster, relevant sensors, power supply unit, image acquisition and lighting unit. Among them, the underwater thruster is controlled by PWM signal sent by ARM integrated control computer, and the other unit equipment is controlled by RS485 communication bus.

2.2.2 Principle of Control System

The function of the underwater robot control system is to send PWM signals through the integrated control computer to control the rotation direction and speed of 8

https://doi.org/10.26549/met.v5i2.8529

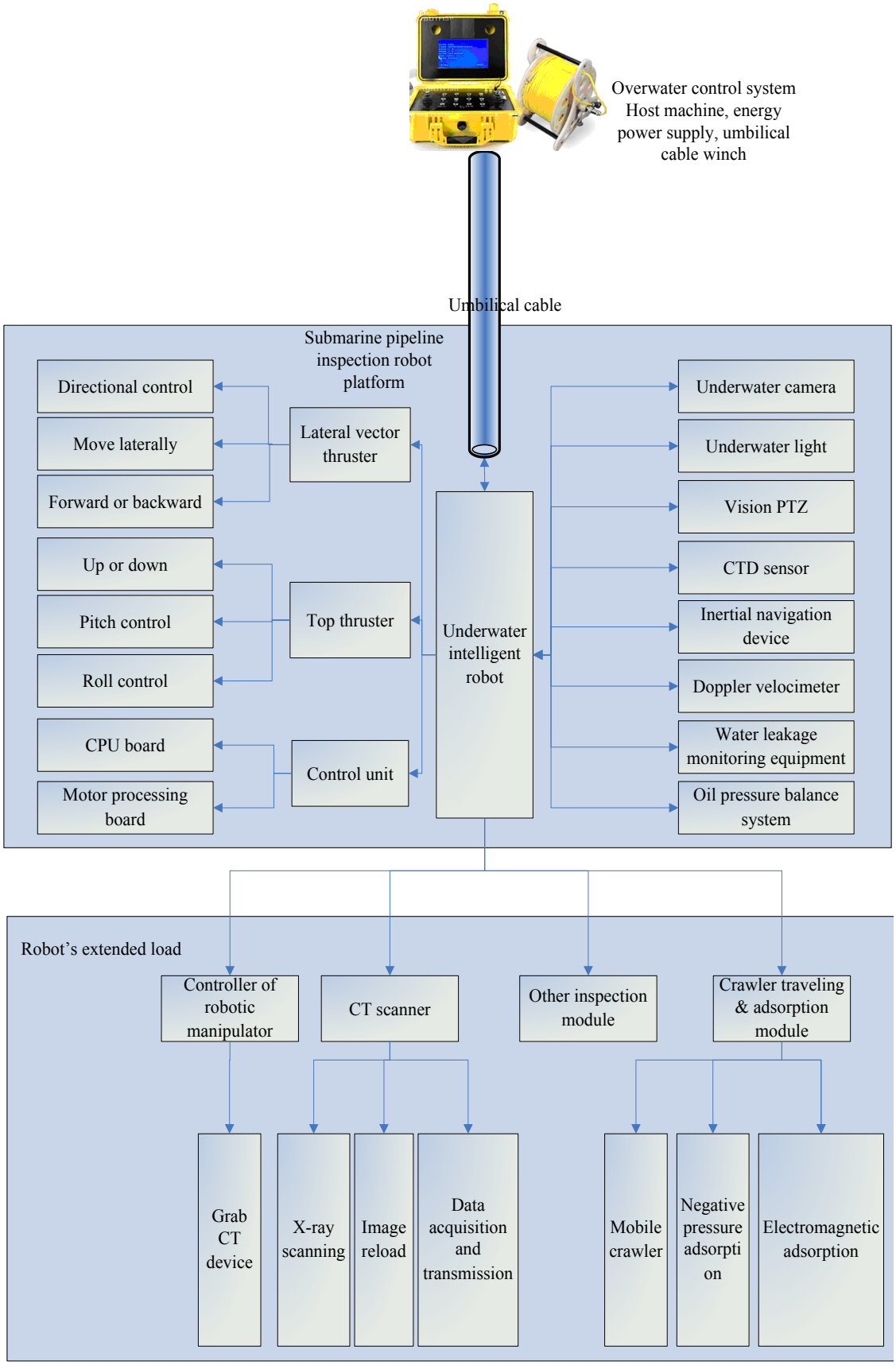

Figure 1. Block Diagram of Robot System

 https://doi.org/10.26549/met.v5i2.8529

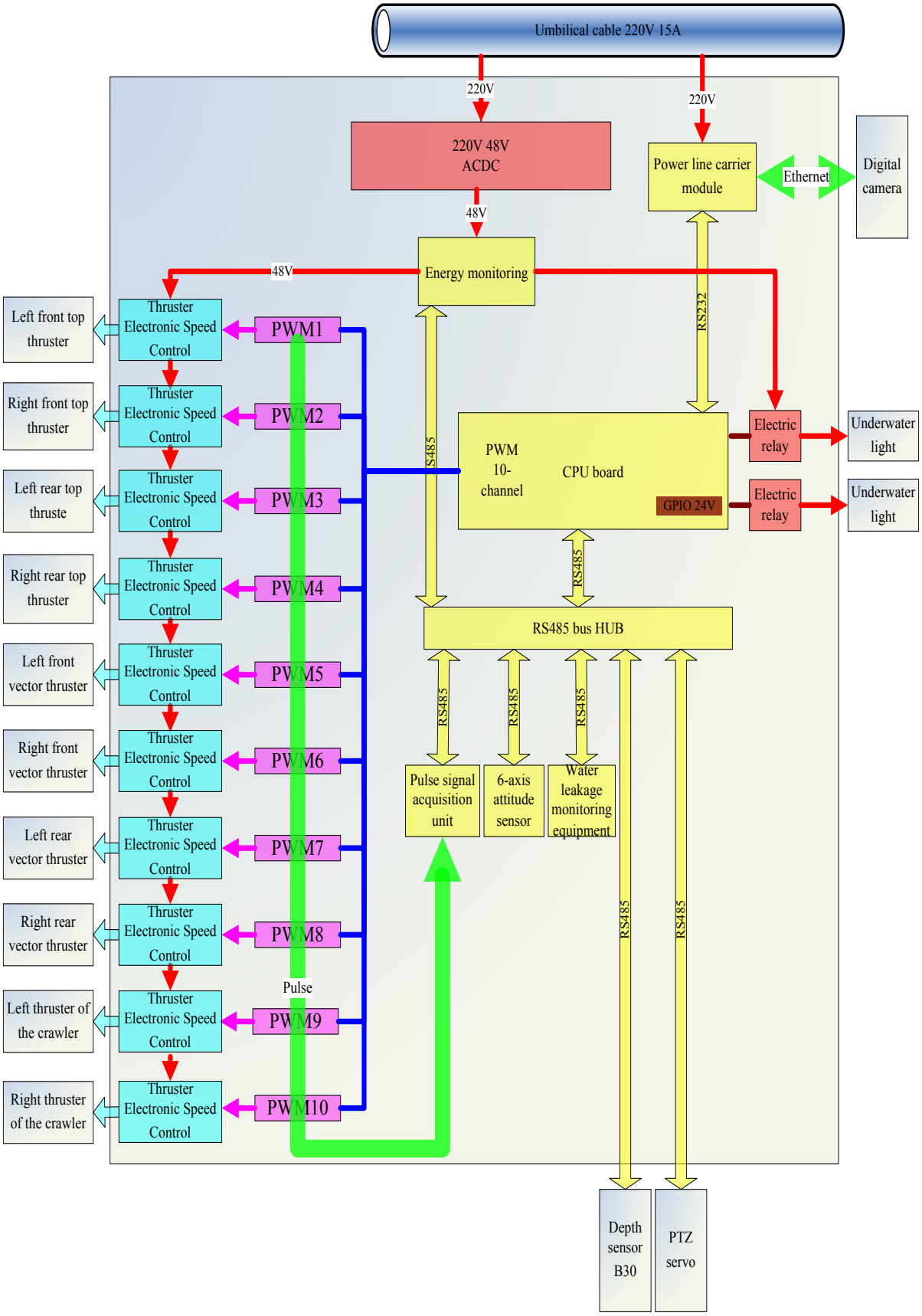

Figure 2. Composition of Control System of Submarine Pipeline Inspection Robot

https://doi.org/10.26549/met.v5i2.8529

thrusters. The external information is sensed by the sensor unit and encapsulated into 485 bus communication format to form a control feedback signal. The integrated control computer analyzes, judges and processes the control feedback signal, and modifies the control law, to make the whole underwater robot move towards the expected direction and speed. The installation position of thrusters on the robot platform is shown in Figure 3, with a total of 8 thrusters, including 4 vertical thrusters on the top and 4 vector thrusters in the transverse direction. Some or all of vertical and vector thrusters work with one another to complete the 6-DOF motion of the robot.

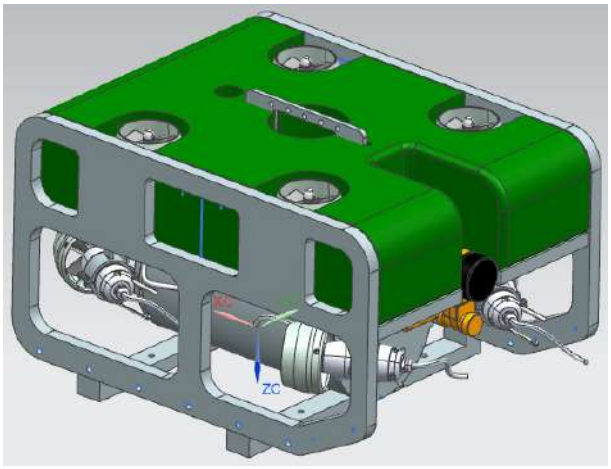

Figure 3. Position of the Thruster Installed in the Underwater Robot

2.3 Design of Non-invasive Submarine Pipeline Inspection System

2.3.1 CT Scanner

The inspection technology of submarine pipeline is mainly used to determine the change of pipeline wall thickness, and the influencing factors mainly include hydrates, wax precipitation, gravels or asphaltene [17]. We mainly adopt the non-invasive submarine pipeline inspection technology — CT scanning technology, which can detect the changes in the wall thickness of different types of pipelines such as riser pipe, insulating pipe and pipe bundle without interrupting the normal operation and production of oil and gas pipeline [18,19], and can also detect the state and relevant parameters of flowing substances such as wax, asphaltene and hydrates [20] inside the pipeline.

The CT scanner designed and manufactured (Figure 4) is composed of the mechanical structure, computer system and CT scanning system.

Figure 4. CT Scanner for Submarine Pipeline

(1) Mechanical structure

Support frame: during operation, it can be wrapped and fixed at the periphery of submarine pipeline to provide support for equipment moving on the pipeline.

ROV connection structure: extend out the robotic manipulator to move and grab the inspection equipment.

(2) CT scanning system

Ray: X-ray

Detector: scintillator photoelectric diode detector is used, with high geometric efficiency.

Power unit for the scanning system: mainly consist of mechanical drive shaft, encoder, motor, shift control board, servo amplifier, etc.

(3) Computer system

Data acquisition and transmission system: connect with overwater analysis system to realize data interaction and transmission.

Image reconstruction and analysis system (Figure 5): mainly consist of system motherboard, special control board, display, array processor, copying machine, etc. It is used to complete synchronous acquisition of CT data and image reconstruction.

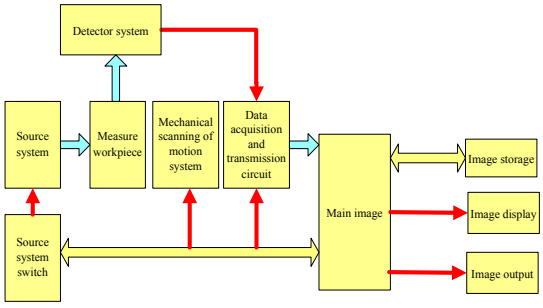

Figure 5. Image Reconstruction and Analysis System

https://doi.org/10.26549/met.v5i2.8529

2.3.2 Pipeline Inspection Principle

The submarine pipeline scanner adopts the CT principle (Figure 6), uses precisely collimated X-rays and highly sensitive detectors to rotate around the submarine pipeline for continuous section scanning, and realizes 360° rapid scanning imaging. Pipeline inspection adopts the fifth generation of CT scanning technology, namely multi-source multi-detector scanning technology [18]. The radiation source and detector are distributed at an angle of 120 degrees. The oil pipeline is in a static state during the inspection, and the radiation source and detector move rapidly along the axial direction of the pipeline.

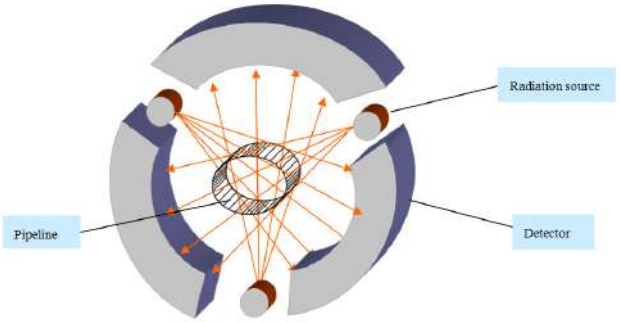

Figure 6. CT scanning schematic diagram of pipeline

2.4 Design of Underwater Negative Pressure Structure

When the working surface of the submarine pipeline inspection robot is not magnetic material, and the magnetic adsorption does not exist, the robot attracts onto the working surface by thrusters. Negative pressure adsorption (Figure 7) is mainly completed by four top thrusters in the floating body of the underwater robot. The thrusters rotate in the adsorption mechanism, and the sealing strip slows down the inlet water velocity, thus forming a throttle mechanism. During operation, due to the water absorption of the thruster, a pressure difference is formed inside and outside, and the internal pressure is less than the external pressure, thus making the robot attach onto the surface. The adsorption force depends on some factors such as the rotational speed of the thruster, and the distance between the sealing strip and the wall. The rotational speed of the thruster can produce the propulsive force towards the surface. Meantime, the higher the rotational speed, the greater the flow of discharged water, the greater the internal and external pressure difference, and the stronger the adsorption force.

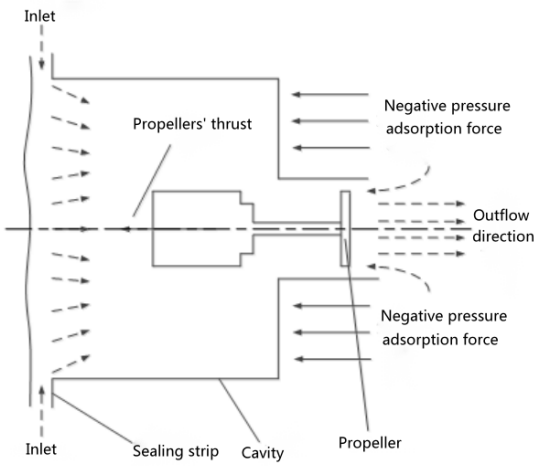

Figure 7. Principle of negative pressure generated by rotation of thrusters

2.5 Design of Underwater Magnetic Adsorption Structure

Magnetic adsorption is mainly to install the third generation of rare earth NdFeB N45 permanent magnet in the robot's crawler (Figure 8 and Figure 9). It adopts the design of type B magnetic circuit. Its magnetic circuit structure has small magnetic resistance, small magnetic leakage and stronger adsorption, so as to ensure the stable adsorption of magnetic blocks on the hull surface. During the moving process, to ensure on damage to the magnet damaged during repeated attraction to and separation from the hull, neoprene blocks are installed on the side surface of the magnetic circuit device to protect the magnet structure, increase the sliding friction coefficient and prevent skidding.

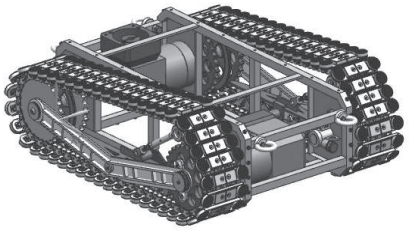

Figure 8. Schematic diagram of underwater intelligent robot platform attracting onto adsorbale tank

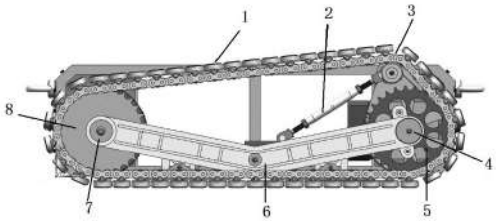

https://doi.org/10.26549/met.v5i2.8529

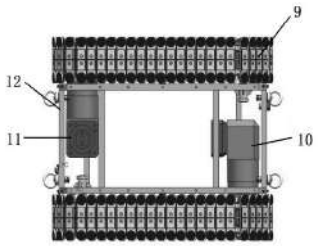

Figure 9. Top View of the Structure of Underwater Intelligent Robot Platform Attracting onto Mobile Crawler
1. Adsorption unit 2. Tension mechanism 3. Chain 4. Driving shaft 5. Driving wheel 6. Support structure 7. Driven shaft 8. Driven wheel 9. Crawler 10. Motor and deceleration structure 11. Fixed block 12. Left and right connecting plates

3. Experiment and Data Analysis

The upper right part of the control interface of the robot's upper computer (Figure 10) is the display area of various status information of the underwater robot (including CT equipment status, ROV operation status, lighting status, image status, etc.), you can click the button control to set some parameters such as the data saving, saving path, saving data start and stop, and communication rate. The lower right part of the control interface is the thruster control area. You can select different operation status, and then drag the progress bar to set the input power of each thruster.

Figure 10. Overwater Control Interface

The upper left part of the control interface is the real-time data recording and saving status of the picture taken by the underwater camera, and information collected by serial communication rocker and displayed in the human-computer interaction interface of the upper computer, and video can be recorded. The lower left part is the overwater analysis system area of CT scanning equipment, which can monitor the pipeline status in real time, store the scanned image in real time and make a judgment. During the inspection and scanning of submarine pipeline, the robot grabs the CT scanner (Figure 11) and places it at the pre-excavated exposed submarine pipeline, the support structure wraps the submarine pipeline, the scanning system starts to scan and inspect the oil and gas pipeline, and the collected information will be transmitted to the ground through wires for data interpretation. (internal pipeline detection image shown in Figure 12, comparison of internal filler detection images with the real object shown in Figure 13, and comparison of hydrate detection images with the real object shown in Figure 14).

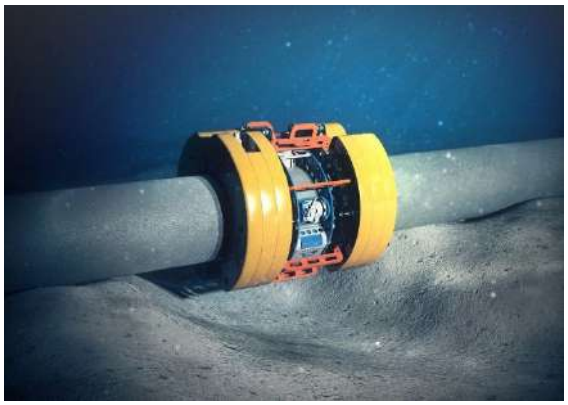

Figure 11. Working State of Pipeline CT Scanning

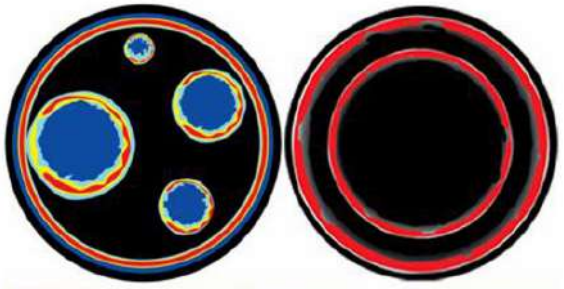

Figure 12. Internal Pipeline Detection Image

Figure 13. Pipeline's Internal Filler Detection Image

Figure 14. Hydrate Detection in Coated Pipes

https://doi.org/10.26549/met.v5i2.8529

4. Conclusions

Different from alternative technologies such as ultrasonic and pulsed eddy current, the non-invasive submarine pipeline inspection robot based on CT technology is a major breakthrough in submarine pipeline inspection. Using the CT scanning technology of submarine pipeline, the oil company can carry out the non-invasive inspection of complex submarine oil pipeline (including ordinary pipes, riser pipes and pipe bundles in the pipeline) from the outside for the first time, to ensure the safe operation of the pipeline. Furthermore, this technology fundamentally solves the problem that during the use of pipeline internal inspection equipment, the tool is easily blocked or stuck, affecting normal production, and meantime solves the problem of inconvenient inspection after pipeline laying. The ROV can be quickly fixed on the outside of the pipeline, the normal production will be not affected during the inspection process, and the operation equipment will not be affected by the external protective layer of the pipeline because there is no need to remove the protective layer of the pipeline during the inspection process, thus eliminating the risk of corrosion caused by removing the coating. The online real-time communication system can quickly obtain the pipeline status information, with high automation, so it is convenient for engineers to know the pipeline dynamics in time, so as to ensure the pipeline integrity and transportation safety.

The international offshore oil pipeline inspection market is mature and the market demand is huge, but the market is basically controlled by European and American countries. China has just started in this industry, but the market demand is increasing. In the near future, the market will become a large market of RMB100 billion. The design and research in this paper fills the gap in the field of offshore pipeline inspection technology in China, and the technology will be widely used in future.

References

[1] Meng Wei. How we ensure the safety of "energy vessel" – revelation of pipeline anti-corrosion and inspection technology[J]. Petroleum Knowledge, 2016, 000 (005): 22-25.

[2] Zhang Likui, Huang Chengyi, Li Jianwei, et al. Risk assessment of oil spill of submarine oil transmission pipeline in Bohai Bay[J]. Ocean Development and Management, 2015, 32 (8): 96-100.

[3] Wang Xiaoping. Overview of offshore oil and gas pipeline inspection technology[C]. China Petroleum and Chemical Automation Annual Conference, 2015.

[4] Zheng Qiuming, Xuan Yingjie. Case analysis of submarine pipeline maintenance[J]. Architectural Engineering Technology and Design, 2018, 000 (014): 933, 918.

[5] Xiao Zhikang, Chi Hongfu, Ai Wanzheng. Causes and prevention of submarine pipeline damaged by anchoring operation[J]. Shipping Management, 2017, 039 (012): 4-6.

[6] Bie Qin, Zheng Yunping, Fu Min, et al. Leakage detection technology and its development trend of oil and gas transmission pipeline at home and abroad[J]. Petroleum Engineering Construction, 2007 (03): 6+29-33.

[7] Zeng Jiangning, Xu Xiaoqun, Shou Lu, et al. Ecological risk of oil spill from submarine oil pipeline and its preventive countermeasures[J]. Ocean Development and Management, 2007 (03): 122-125.

[8] Xu Xuewu. In-line inspection and corrosion analysis for submarine pipeline from Weizhou 11-1 to 12-1PAP[J]. Corrosion & Protection, 2015 (07): 643-647.

[9] Yu Xizhi. CNOOC's annual performance may be even worse due to four-time leaks in the year[J]. Construction Machinery and Equipment, 2013.

[10] Dong Xue. Discussion on problems related to offshore oil equipment[J]. China Chemical Trade, 2015, 007 (025): 170.

[11] Feng Qingshan, Zhang Hailiang, Wang Chunming, et al. Advantages of three-axial high-resolution magnetic flux leakage inspection technology and its application status[J]. Oil & Gas Storage and Transportation, 2016, 035 (010): 1050-1054.

[12] LIAO Xiaoxiao, ZHOU Shaoqi, LIU Shengqun. Finite element simulation of three axis AC magnetic flux leakage detection[J]. Automation & Instrumentation, 2015.

[13] Yang Lijian, Zhang Xiaodan, Gao Songwei, et al. Research on the propagation characteristics of ultrasonic wave in the detection of pipeline coating[J]. Journal of Electronic Measurement and Instrumentation, 2018, 032 (001): 9-18.

[14] Sun Zheng, Li Yongqian, Yang Jinxu, et al. Thickness gauging equipment for ILI of pipelines using EMATs[J]. China Measurement & Test, 2017, 043 (002): 69-72.

[15] Liu Zhuohui. Three dimensional simulation and experimental verification of far-field eddy current testing technology for ferromagnetic pipeline [J]. Petro & Chemical Equipment, 2016 (8): 71-74.

[16] Wei Y, Hongxin M A, Bin G, et al. Inline inspection on riser of submarine pipeline based on remote field eddy current detection technique[J]. Oil & Gas Stor-

https://doi.org/10.26549/met.v5i2.8529

age and Transportation, 2015.
[17] Su Xin. Research on wax deposition and pipeline cleaning cycle of submarine waxy crude oil pipeline[D]. Southwest Petroleum University, 2015.
[18] Qi Xiaojie, Zheng Ze, Wang Jianming, et al. Damage and nondestructive testing of petrochemical pressure pipeline[J]. Consume Guide, 2018, 000 (043): 168.
[19] John, Hoffman, Nastaran, et al. Technical Note: Design and implementation of a high-throughput pipeline for reconstruction and quantitative analysis of CT image data[J]. Medical Physics, 2019.
[20] Zhang GuanLiang, Zhang Zubo, Liu Qingjie, et al. Study on effects of polymer flooding on layered heterogeneous reservoirs using CT scanning[J]. Petroleum Geology and Recovery Efficiency, 2015, 022 (001): 78-83.

 https://doi.org/10.26549/met.v5i2.8529

SYNERGY PUBLISHING PTE. LTD

Modern Electronic Technology

https://ojs.s-p.sg/index.php/met

Research on Thermal Management Control Strategy of Electric Vehicle Liquid Cooling Battery Pack

Zhenhua Li*

Sangdun New Energy Technology Co., Ltd., Xiangtan, Hunan, 411202, China

ARTICLE INFO

Article history
Received: 5 October 2021
Revised: 12 October 2021
Accepted: 18 October 2021
Published Online: 25 October 2021

Keywords:
Electric vehicle
Power battery liquid cooling system
Computational fluid dynamics
Analogue simulation

ABSTRACT

Due to the risk of thermal runaway in the charging and discharging process of a soft packed lithium battery pack for electric vehicles, a stamping channel liquid cooling plate cooling system is designed, and then the heat dissipation problem of the battery pack is solved through reasonable thermal management control strategy. Using computational fluid dynamics simulation software star-CCM+, the thermal management control strategy is optimized through simulation technology, and the temperature field distribution of battery pack is obtained. Finally, an experimental platform is built, combined with experiments, the effectiveness of the thermal management control strategy of the cooling system is verified. The results show that when the battery pack is in the environment of 25℃ , the maximum temperature of the cooling system can be lower than 40℃ , the maximum temperature difference between all single batteries is within 5℃ , and the maximum temperature difference between inlet and outlet coolant is 3 ℃ , which can meet the heat dissipation requirements of the battery pack and prevent out of control heat generation.

1. Introduction

At present, due to the problems of environmental protection and energy security, the state vigorously develops new energy electric vehicles, and the core technology of electric vehicles is lithium-ion battery pack. How to prevent the battery pack from thermal runaway and spontaneous combustion under charge and discharge conditions is an urgent research hotspot. When the lithium-ion battery pack is working, a large amount of heat is generated due to continuous high current charging and discharging. If the heat is not dissipated in time, the excessive temperature and temperature difference will seriously affect the power performance and service life of the electric vehicle [1]. Aiming at the risk of thermal runaway in the charging and discharging process of a soft packed lithium battery pack for electric vehicles, a stamping channel liquid cooling plate cooling system is designed, and then the heat dissipation problem of the battery pack is solved through reasonable thermal management control strategy; Using the computational fluid dynamics simulation software star CCM +, the thermal management control strategy is optimized through the simulation technology. Finally, the experimental platform is built. Combined with the experiment, the effectiveness of the thermal management control strategy of the cooling system is verified.

2. Battery Pack Cooling System Design

The battery pack consists of 20 modules, which are

**Corresponding Author:*
Zhenhua Li,
Sangdun New Energy Technology Co., Ltd., Xiangtan, Hunan, 411202, China;
Email: 1957876517@qq.com

https://doi.org/10.26549/met.v5i2.8596

placed in parallel in upper and lower layers, with 8 columns in the lower layer and 2 columns in the upper layer; each module contains 32 17.5ah soft packed lithium batteries, which are formed in series and parallel. The battery pack adopts the stamping channel liquid cooling plate cooling system, which is mainly composed of heat conducting silica gel pad, inlet and outlet water pipe and stamping liquid cooling plate; the three stamping liquid cooling plates are connected in series. The heat is transferred between the liquid cooling plate and the battery module through the heat conducting silica gel pad, and the coolant is 50% ethylene glycol water mixed solution. See Figure 1 and Figure 2.

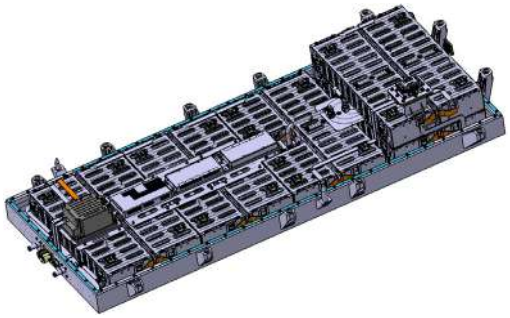

Figure 1. battery module system

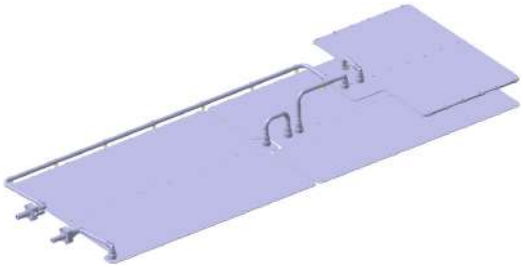

Figure 2. liquid cooling plate cooling system

3. Simulation Calculation of Battery Pack Cooling System

3.1 Governing Equations of Computational Fluid Dynamics

In the process of fluid flow, three conservation laws are observed: the law of mass conservation, the law of momentum conservation and the law of energy conservation. In computational fluid dynamics [2,3], there should be: mass conservation equation, momentum conservation equation and energy conservation equation.

(1) Mass conservation equation

$$\frac{\partial \rho}{\partial t} + div(\rho U) = 0 \quad (1)$$

Where ρ is the fluid density; U is the velocity vector.

(2) Momentum conservation equation

$$\frac{\partial(\rho u)}{\partial t} + div(\rho u U) = div(\mu gradu) - \frac{\partial p}{\partial x} + S_u \quad (2)$$

$$\frac{\partial(\rho v)}{\partial t} + div(\rho v U) = div(\mu gradv) - \frac{\partial p}{\partial y} + S_v \quad (3)$$

$$\frac{\partial(\rho w)}{\partial t} + div(\rho w U) = div(\mu gradw) - \frac{\partial p}{\partial z} + S_w \quad (4)$$

Where ρ is the fluid density; u、v、w are the velocity components of velocity vector U in x、y、z directions respectively; μ is hydrodynamic viscosity; S_u S_v S_w are the generalized source term of the momentum conservation equation.

(3) Energy conservation equation

$$\frac{\partial(\rho T)}{\partial t} + div(\rho U T) = div\left(\frac{k}{C_p} grad T\right) + S_T \quad (5)$$

Where k is the heat transfer coefficient of the fluid; C_p is the specific heat capacity of the fluid; S_T is viscous dissipation term.

(4) Differential equation of heat conduction in battery

$$\rho C \frac{\partial T}{\partial t} = \lambda_x \frac{\partial^2 T}{\partial x^2} + \lambda_y \frac{\partial^2 T}{\partial y^2} + \lambda_z \frac{\partial^2 T}{\partial z^2} + q \quad (6)$$

Where ρ is the cell micro cell density; C is the specific heat capacity of micro cell of battery; λ is the thermal conductivity of battery micro element; q is the heat generation rate of battery micro element.

3.2 Thermal Management Simulation Strategy

Working condition 1: Under the ambient temperature of 25 ℃, the initial temperature of the system is 26.5 ℃, the coolant is not turned on. The battery pack 1C is charged (the heating power of the cell is 2W), until the maximum temperature at the probe point rises to 36 ℃.

Working condition 2: When the maximum temperature of the probe point rises to 36 ℃, battery pack 1C continues to charge (the heating power of the cell is 2W), and at the same time, turn on 15 ℃ coolant 10L/min until the total charging time is 3243S.

Working condition 3: When the total charging time is 3243s, the battery pack 1C-0C continues to charge (the heating power of the cell is 0.38W), and the 15 ℃ coolant is opened for 10L/min. The battery pack 1C-0C current drop charging time is 1440S.

Working condition 4: When the 1C-0C current drop charging of the battery pack is completed, the battery pack starts to stand. At the same time, open 15 ℃ coolant 10L/min until the maximum temperature of the cell probe point is reduced to 30 ℃. It takes 405S for the maximum temperature of the battery pack to drop to 30 ℃ from the beginning of stand.

 https://doi.org/10.26549/met.v5i2.8596

Working condition 5: When the maximum temperature of the probe point of the cell is reduced to 30 ℃ , the battery pack continues to stand for 75s, and the 15 ℃ coolant 10L/min is closed at the same time.

Working condition 6: After standing, turn off 15 ℃ coolant 10L/min at the same time, battery pack 1C discharge (heating power of cell is 2W), and it takes 1710S until the maximum temperature at the probe point rises to 38 ℃ .

Working condition 7: When the maximum temperature of the probe point of the cell rises to 38 ℃ , turn on the 15 ℃ coolant for 10L/min, and the battery pack 1C continues to discharge for 1890S (heating power of the cell is 2W) until the discharge of the cell is completed.

Working condition 8: When the 1C discharge of cell is completed, continue to turn on 15 ℃ coolant for 10L / min, and the battery pack stands for 240S.

Working condition 9: After the stand of battery, battery pack 1C charge for 1800S (heating power of battery cell is 2W) and keep the 15℃ coolant open for 10L / min.

3.3 Boundary Condition

Between the box body and the external environment is convective heat exchange; between the coolant and liquid cooling plate is convective heat exchange and heat conduction; between the battery module and heat conducting silica gel, heat conducting silica gel and liquid cooling plate are heat conduction, and the rest parts and the air in the box body are natural convective heat exchange. See Table 1 for material property parameters of each part of the simulation model.

Table 1. material parameters of each part of the model

material	density kg/m^3	specific heat capacity $J/(kg*K)$	thermal conductivity $W/(m*K)$
aluminum alloy	913	2710	201
foamed silica gel	820	324	0.04
EVA foam	850	101	0.085
ABS+PC	1150	1300	0.24
coolant	1062	3305	0.418
battery cell	1933	1080	axial 0.66, radial 22.3
air	1.279	1006	0.024

3.4 Analysis of Simulation Results

As shown in Figure 3, along the flow path of the coolant, the temperature of the liquid cooling plate increases gradually, and the temperature of the battery pack also increases gradually. The coolant takes away heat in the process of flow, which also causes the temperature difference between battery packs. In Figure 4, in order to display the temperature difference between different battery packs, 29 temperature detection points are set to monitor the top, middle and bottom temperatures of the battery respectively. In Figure 5, according to the analysis, during the whole working condition, the maximum temperature of the cooling system can be lower than 40 ℃ ; the maximum temperature difference of all arranged probe points is within 5 ℃ , and the maximum temperature difference of inlet and outlet coolant is 3℃ , which can meet the heat dissipation requirements of the battery pack and prevent thermal runaway.

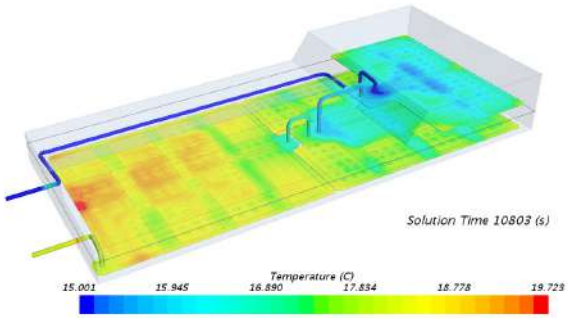

Figure 3. cloud diagram of temperature field of liquid cooling plate

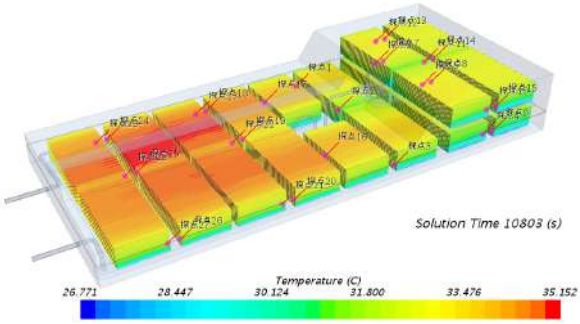

Figure 4. cloud diagram of battery pack temperature field

4. Experimental Verification of Temperature Field of Battery Pack

4.1 Experimental Equipment and Temperature Distribution Scheme

In order to obtain the cooling effect of the battery pack under actual working conditions, an experimental platform needs to be built for testing, as shown in Figure 6. The selection of the detection position of the temperature point is consistent with that in the simulation calculation, which is convenient for comparative analysis. It is proposed to distribute 29 T-type thermocouples on the surface of the battery pack. Figure 7 shows that the charging and discharging system of the power battery is TECHPOW-600, and the water-cooled circulator system is

https://doi.org/10.26549/met.v5i2.8596

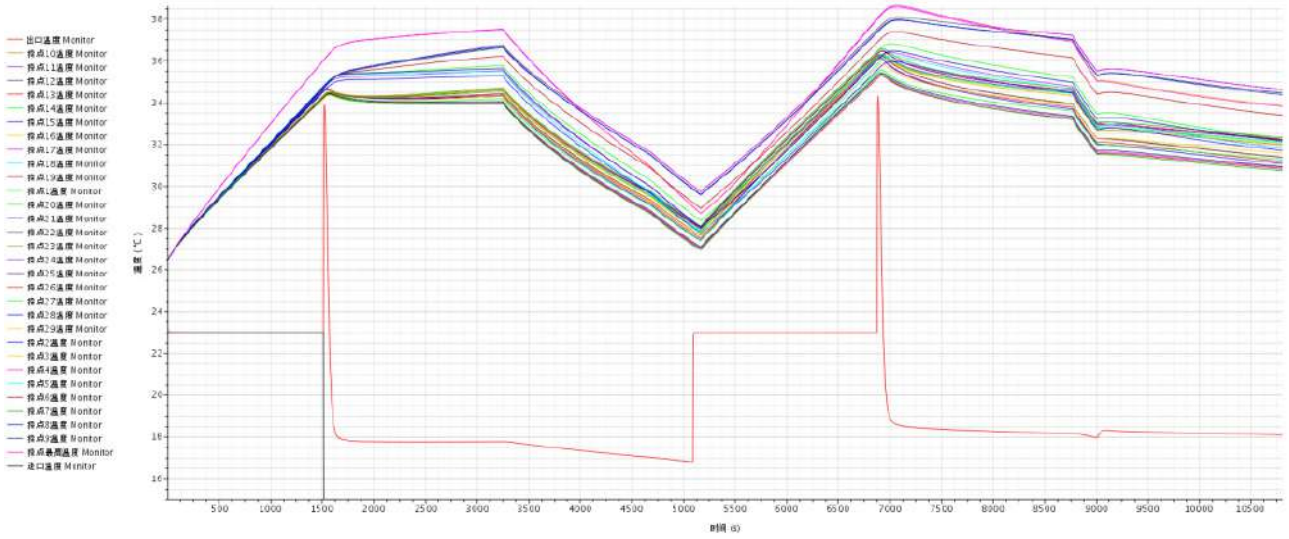

Figure 5. curve of coolant temperature at detection points and outlet

a multifunctional GE522A. After the establishment of the experimental platform, set the coolant inlet temperature to 15 ℃ , and adjust the temperature of the constant temperature chamber to 25℃ , and start the charging and discharging equipment to charge and discharge the battery pack according to the thermal management simulation strategy.

Figure 6. experimental platform

Figure7. charging and discharging equipment

4.2 Analysis of Experimental Results

Figure 8 is the curve of each temperature sensor monitored during the experiment, and Figure 9 is the temperature of each sampling point of the battery pack at the time 3376S during the experiment.

Figure 8 shows that the experimental results are basically consistent with the simulation data. The battery pack does not have too high temperature points, and the temperature distribution is in good consistency. As can be seen from Figure 9, the highest temperature point is T3 sampling point, which is located at the bottom of the lower battery, and the temperature is 35.8 ℃ ; The lowest temperature point is T12, which is located in the middle of the upper battery near the water inlet side; and the temperature is 30.8 ℃ . The maximum temperature difference of each monitoring point of the battery pack is 5℃ .

5. Conclusions

Aiming at the risk of thermal runaway in the charging and discharging process of a soft packed lithium battery pack for electric vehicles, a stamping channel liquid cooling plate cooling system is designed, and then the heat dissipation problem of the battery pack is solved through reasonable thermal management control strategy. Using the computational fluid dynamics simulation software star CCM+, the thermal management control strategy is optimized by simulation technology, and the temperature field distribution of the battery pack is obtained. Finally, an experimental platform is built to verify the effectiveness of the thermal management control strategy of the cooling system. The results show that when the battery pack is in the environment of 25℃ , the maximum

 https://doi.org/10.26549/met.v5i2.8596

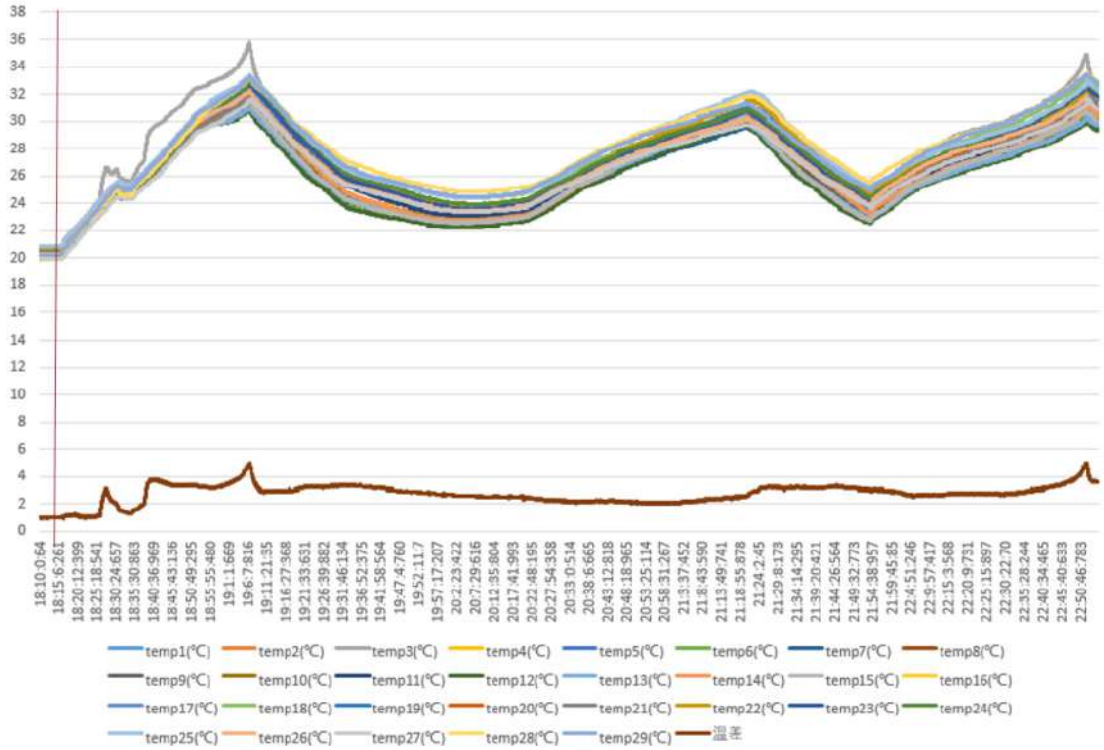

Figure 8. curve of each sampling point during the experiment

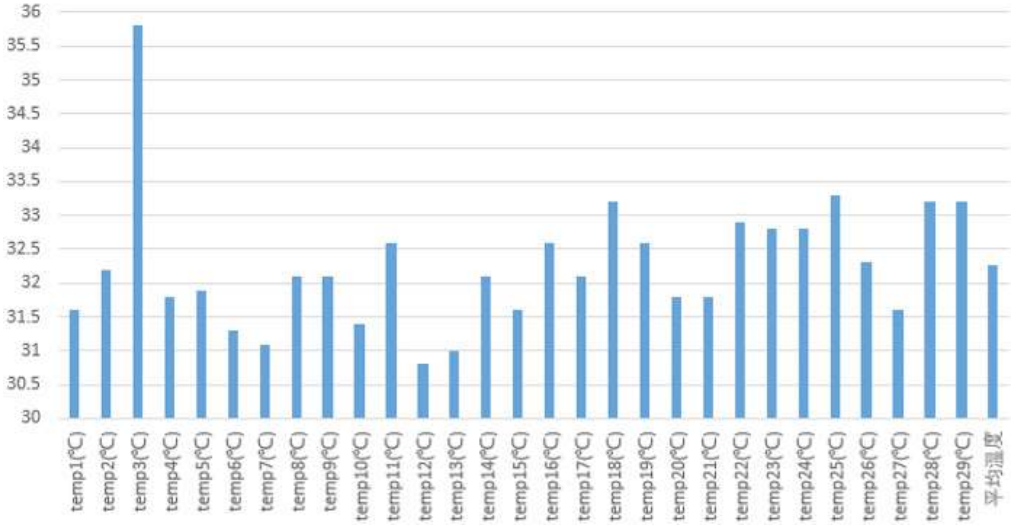

Figure 9. temperature of each sampling point at the time3376S

temperature of the cooling system can be lower than 40℃ , and the maximum temperature difference between all single batteries is within 5 ℃ , and the maximum temperature difference between inlet and outlet coolant is 3℃ , which can meet the heat dissipation requirements of the battery pack and prevent thermal runaway.

References

[1] Zhao Yongjin, Liao Ping, Zhu Jianxin. Research on the cooling system of nickel-hydrogen (Ni-MH) battery package for hybrid electric vehicle [J]. Chinese Journal of Power Sources, 2019, 43(6), 1010-1012.

[2] Zhang Xin, Wang Tong, Xu Haigang. Simulation analysis of temperature of square power lithium-ion battery based on parallel air-cooling [J]. Chinese Journal of Power Sources,2019, 43(3),426-428.

[3] Du Minghui, Zheng Xinwei, Jiang Zhenwen. Analysis of influencing factors on heat dissipation performance on liquid-cooled of electric vehicle battery module [J]. Guangdong Chemical Industry, 2018,45(16),48-50.

https://doi.org/10.26549/met.v5i2.8596

About the Publisher

Synergy Publishing Pte. Ltd. (SP) is an international publisher of online, open access and scholarly peer-reviewed journals covering a wide range of academic disciplines including science, technology, medicine, engineering, education and social science. Reflecting the latest research from a broad sweep of subjects, our content is accessible worldwide – both in print and online.

SP aims to provide an analytics as well as platform for information exchange and discussion that help organizations and professionals in advancing society for the betterment of mankind. SP hopes to be indexed by well-known databases in order to expand its reach to the science community, and eventually grow to be a reputable publisher recognized by scholars and researchers around the world.

SP adopts the Open Journal Systems, see on http://ojs.s-p.sg

Database Inclusion

Asia & Pacific Science Citation Index

Creative Commons

China National Knowledge Infrastructure

Google Scholar

Crossref

MyScienceWork

SYNERGY
PUBLISHING PTE. LTD.
Tel: +65 65881289
E-mail: contact@s-p.sg
Website: ojs.s-p.sg

ISSN 2591-7110
02
9 772591 711214